Response to reviews of acp-2019-977 by Botía et al.

Comment from Referee 2 - Received on February 19/2020

The format in which the response is addressed is:

1. Black text shows comment of referee. Comments are numerated as RC2.1, for the comment 1 of referee 2. The page and line referred to by the referee are also shown.

2. Blue text shows the author's response and it has the same logic for numeration (e.g. AR2.1).

3. Red text shows the changes to the manuscript.

4. *Italics, underline and red text shows citations from the manuscript*.

General Comments

[**RC2.1**] I suggest to re-structured the Results chapter. At moment, the different sub-sections include both results and discussion, and in some cases even methodology. Moreover, they are too lengthy and sometimes the reader loss the story line. So, I suggest to separate text related to results and discussion in two different sections. The chapter 3.3 and related sub-sections are mainly Discussions and not really presenting results. Finally, I see the needs to reduce the length of the text, as also suggested by the other Reviewer.

[**AR2.1**] We appreciate the referee's comments and believe shortening the text will be beneficial for the manuscript. The separation of Results and Discussion was done and we refer the referee to the revised manuscript. Sections 3.3.1 and 3.3.2 were added as a part of the Discussion, yet **Section 3.3.3 Rejecting Biomass Burning Influence on positive CH_4 gradients** was left in the Results. This Section was renamed as **Rejecting biomass burning and Amazon river as sources of the positive CH_4 gradients** because the part in which we discard the Amazon river as source of the positive CH_4 gradients was added. The motivation for this is that this part is based on analysis of our data. Furthermore, and as we stated to the referee 1, Figure 12 has been updated as more Black Carbon data became available in the meantime. The new time series extends from June 2013 to May 2018. This information has been updated in the methodology section accordingly.

[**RC2.2**] Most of the events associated with positive CH4 gradient are associated with strong thermal inversions, low vertical mixing and decoupled regimes. I believe the decoupling happen somewhere between the canopy layer and the 79 m height. Could the authors see any systematic wind direction difference between the two layers? This would be a clear evidence supporting the idea of decoupling layer (see Alekseychik et al., 2013) for an example of such analysis related to a boreal forest in Finland).

[**AR2.2**] Thanks for your suggestion, we have analyzed our dataset from this perspective. First, is worth recalling that our CH_4 inlet is at 79 m and the closest sonic anemometer is at 81 m, we have stated this in P11-l24: *The heights of the highest sonic anemometer and the highest air inlet for CH_4*

mixing ratio measurements differ by two meters, with the former at 81 m and the latter at 79 m. We assume that the effect of the two meters can be neglected and thus interpret all the 81 m data as valid for 79 m.. We found a systematic difference in wind direction under CH_4 enhancement events but also, when they do not occur (see Fig. 1). This plot was based on Figure 5 in Alekseychik et al. (2013), the reference suggested by referee 2. This indicates that nighttime conditions at ATTO are often decoupled showing wind direction differences between levels. Decoupling conditions of the air within and above the canopy during nighttime were first described by Shuttleworth (1985) and at the ATTO site were mentioned by Andreae et al. (2015). Here we show that the decoupling holds from 19 m to 26 m but at 42 m the wind direction has a similar distribution to that at the upper level. It is important to note here that under positive CH_4 gradients in addition to the wind direction difference, there are marked differences in net radiation, sensible heat flux, friction velocity and virtual potential gradient as depicted by Figure 9 of the manuscript. As this analysis does not influence our results we have decided to not include this plot in the revised manuscript.
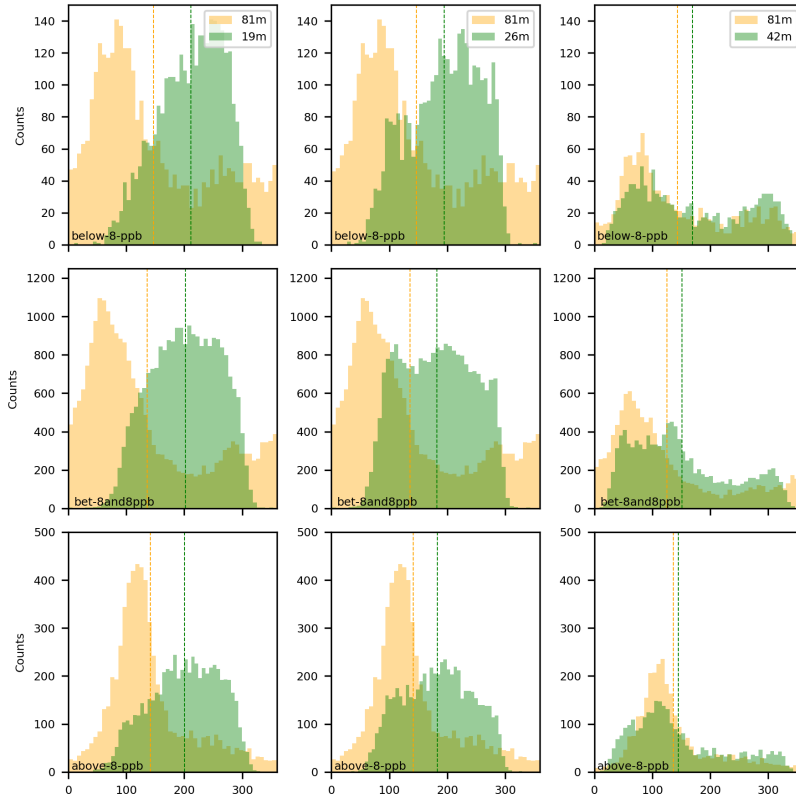
Figure 1: Wind direction distribution at 81 and 19 m levels (left column), at 81 and 26 m (middle column) and at 81 m and 42 m (right column). The upper row shows the below-8-ppb class, the middle row the between -8 and 8 ppb class and the lower row the above-8-ppb class. The vertical lines indicate the mean values for each distribution. See the manuscript for further details on our nighttime definition and the last comment in this document. Note that the distribution is limited to the availability of data at both levels, this is why the comparison between 81 m and 42 m levels differ from the others in the same row.

[**RC2.3**] The authors suggest the nighttime CH4 enhancement above the canopy (at 79m) are advected from the Uatumã river by horizontal non-turbulent motion. Assuming this is true, do the authors see also an increase of CO2 mixing ratio at 79m? In fact it is evident that rivers (even in Amazonia region) are also a strong sources of CO2 (authors can easily find few recent papers in literature related to this topic). However, for CO2 the gradient would be still negative due to strong local sources related to nighttime soil respiration.

[**AR2.3**] As the referee states, the CO_2 gradient will always be negative due to very strong nighttime respiration. Therefore, is difficult to identify a CO_2 increase with our gradient approach. We do not discard that an increase in CO_2 could happen, but the magnitude of such enhancement is very often masked by very strong CO_2 signals that are locally produced at lower levels. An example of this is shown on Fig. 2. At the time of CH_4 enhancement (at around 21:00) there is a very small

increase in CO_2 mixing ratios at 79 m and not seen at 24 m, this can be possibly attributed to an enhancement coming from the Uatumã river. However, later in the night a bottom-up strong local signal arrives at 79 m at about 03:00, masking the earlier effect. A short sentence taking into account this comment was added to the revised manuscript. See section 4.1.
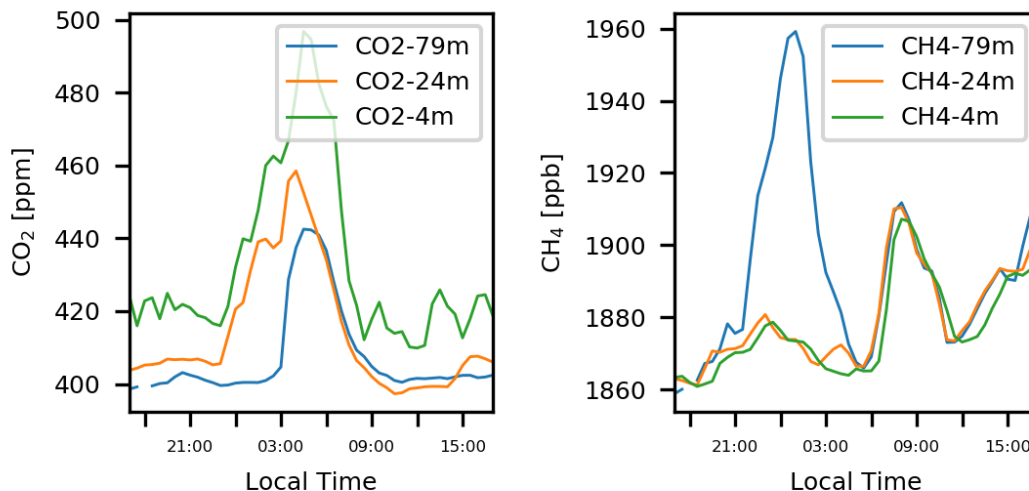

Figure 2: Time series for a 24-hour interval (same as in Fig 6a in manuscript) for CO_2 and CH_4.

Minor Comments

[RC2.4]-P2,l21 and l23: CH4 mixing ratio?

[AR2.4] From this comment, we interpret that the referee is suggesting to define the mixing ratio measure earlier in the text. Since this is a common and well-known measure for concentrations of chemical species in the atmosphere, we believe is not necessary to define it.

[RC2.5]-P2,l34: "...accumulation of CH4 above the canopy..."

[AR2.5] We have corrected the sentence as suggested by the referee.

[RC2.6]-P4,l25-26: I would rephrase as "....wind speed profiles for specific nights, using additional data....".

[AR2.6] Thank you for the comment, we have modified the text accordingly.

[RC2.7]-P5,l26 to P6,l2: This text can go under Discussion.

[AR2.7] Yes, we agree with the comment and have included this part under Discussion.

[RC2.8]-P10,l4-8: This text can go under Methodology, as it is related to how the data were analysed.

[AR2.8] Thanks for the suggestion, the text has been added to the Methods section.

[RC2.9]-Chapter 3.2.2 and Figure 9: I would move this text and figure 9 to Appendix, or even removed from the manuscript. I am not sure about the meaning of friction velocity as surface layer scaling parameter in case of decoupling and/or very shallow NBL. I would rather suggest to look at some stability parameters, like bulk Richardson number (even calculated for different layers) or z/L, which would include both the mechanical forcing related to wind shear as well as the effect of buoyancy, which could act as suppression (stable conditions) or production (unstable conditions) mechanism for turbulent mixing.

[**AR2.9**] We understand the perspective of the referee 2, however we do not think Section 3.2.2 and Figure 9 should be left out of the manuscript nor moved to the Appendix. The main objective of this section was to show the effects of some parameters associated with atmospheric stability, such as sensible heat flux (H) and friction velocity (u_*), on the CH_4 positive gradients. The friction velocity was used here as a direct measure of mechanical turbulence and not as a surface layer scaling parameter. On Figure 9 of the manuscript was shown that the strong CH_4 gradients (above-8-pbb class) were associated with high negative sensible heat flux values and low values of friction velocity. Therefore, for situations with strong CH_4 gradients, it is expected that the Obuhkov length (L) will present smaller values than the other class (below-8-pbb class). In Fig. 3 the z/L values for the two CH_4 classes investigated are shown. As expected, the z/L values were generally higher for the above-8-pbb (since L is lower) than for the below-8-ppb class.
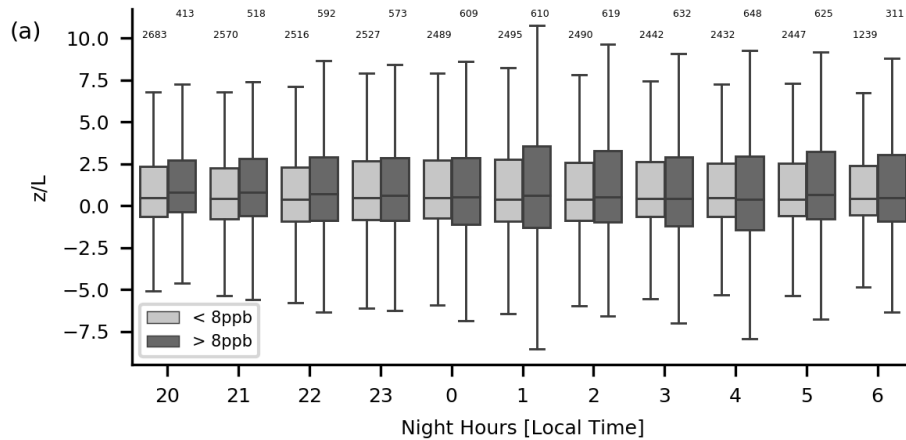

Figure 3: Nighttime evolution of z/L for the two classes analyzed in Section 3.2.2 above-8-pbb and below-8-ppb.

[RC2.10]-P12,l9: Do you mean above-8-ppb CH4 gradients?

[**AR2.10**] Yes. Thanks for pointing this out. The sentence was corrected for clarity.

[RC2.11]-P12,l9: How H is calculated? Have you corrected the kinematic heat flux w'T' for the effect of H2O fluctuations? And if yes, how did you measure the H2O fluctuations? Was a Licor installed at 81m?

[**AR2.11**] In this section we use 30-min averages that are processed in the EddyPro/Alteddy softwares. The correction for the effect of water fluctuations is performed with information from an IRGA (LI-7500A, LI-COR Inc., USA) located at 81 m. We included this in the Meteorological Instrumentation part as: At 81 m molar densities of CO_2 and H_2O are measured with an IRGA (LI-7500A, LI-COR Inc., USA).

[**RC2.12**]-**P12,l12**: The heat fluxes close to zero may even indicate near-neutral atmospheric conditions, and it depends also on the relative magnitude of the wind shear forcing. See my comments above.

[**AR2.12**] We agree with the referee 2, sensible heat fluxes close to zero may also indicate near-neutral conditions. Thus, we interpret the referee's comment about the relative magnitude of wind shear forcing, as a suggestion for an additional argument that can explain the lower sensible heat flux values for the above-8-pbb class. However, as we show on Fig 8 of the manuscript, the probability of having CH_4 gradients above 8 ppb was higher for wind speeds within a range between 2 and 5 m s^{-1} (explicitly stated in P13,l4), so for relatively high wind shear at moderate wind speeds (above 4 m s^{-1}) we could also have methane enhancement events. This is the reason why when presenting the results for sensible heat flux in this part of the manuscript, we limited the analysis to stability and the nocturnal boundary layer height.

[**RC2.13**]-**P13,l8-14**: Can this behavior of the friction velocity profile (indicating actually a momentum flux divergence) be checked and analysed for the present dataset?

[**AR2.13**] Although we don't have friction velocity data for as many levels as Acevedo et al. (2016) had, we have checked this behaviour at 81 m and 46 m for two temporal scales, 30-minute and 1-minute averages. Unfortunately, we only have 1-minute data at both heights for August in 2014, yet the 30-minute record extends from 2013 to 2018 for both heights. The 1-minute data requires to be requested with some time in advance and we are limited to what we have at the moment. We took 46 m as the near-surface level since the canopy is just below 40 m and averaged the friction velocity for different wind speed bins at 46 m. The results of this are shown in Fig. 4. In the decoupled regime described in Acevedo et al. (2016), friction velocity at higher levels is increasingly driven by submeso motions. At ATTO the contribution of submeso motions is less dominant (Acevedo et al., 2014), explaining why we see a negative gradient of friction velocity (Fig. 4) and also why it does not change signs as observed by Acevedo et al. (2016). Our final decision considering that we needed to shorten the manuscript and that this part is not fundamental for the main conclusions, we decided to take these lines [P13,l8-14] out of the revised manuscript.
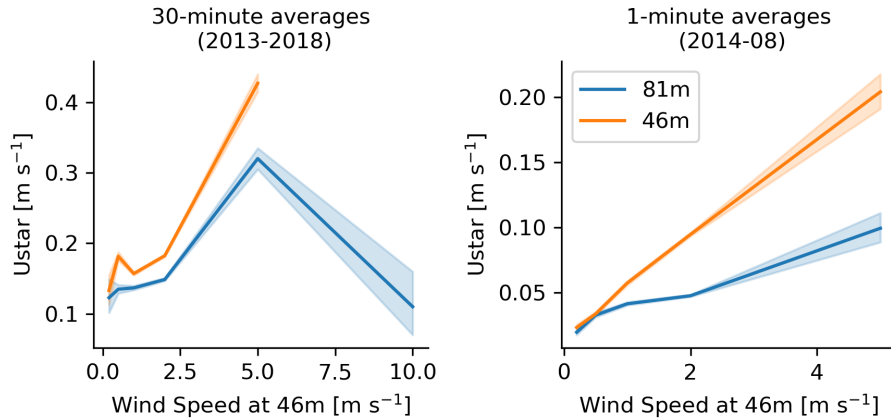
Figure 4: Friction velocity at 81 and 46 m as a function of wind speed at 46 m. Plotted using 30-minute averages (left panel) and 1-minute averages (right panel).

[**RC2.14**]-**P14,l16**: Please explain the difference between regimes 1 and 2.

[**AR2.14**] The main characteristics of regimes 1 and 2 are explained three lines below, (i.e. P14,l19). However, in the revised version we have placed these lines earlier in the text.

[**RC2.15**]-**P14,l25-26**: I was thinking if this drop in the $sigma_w$ the authors see for relatively moderate wind speed, could be related to the fact that 1 min average values are used for such analysis, which may filter out contribution of low frequency (e.g. submeso motions) to the std values.

[**AR2.15**] The 1 min average values follows recent practice in stable boundary layer studies (Mahrt et al., 2013; Acevedo et al., 2016; Stiperski et al., 2019). Moreover, it has been also applied for producing what is commonly known as the "Hockey stick plot" (Sun et al., 2012, Acevedo et al., 2016, 2019 and Mortarini et al., 2019), Figure 10 of the manuscript. Furthermore, the contribution from submeso motions, if not filtered using a small averaging window, may produce unpredictable large-scale contributions to vertical fluxes, increasing the variability associated with most of the quantities (Mahrt et al., 2013; Stefanello et al., 2020). Therefore, we believe that for our purpose –analyzing the positive gradients from the hockey stick plot perspective– we had to filtered out submeso motions to purely target turbulent scales. Nevertheless, under very stable conditions the time-scale of turbulent motions can decrease (Oliveira et al., 2018), thus the 1-minute averages can still be affected by submeso motions. In Fig. 5 we have used a larger averaging window (5 minutes) and we still see the drop in $sigma_W$ and the same wind speed threshold.
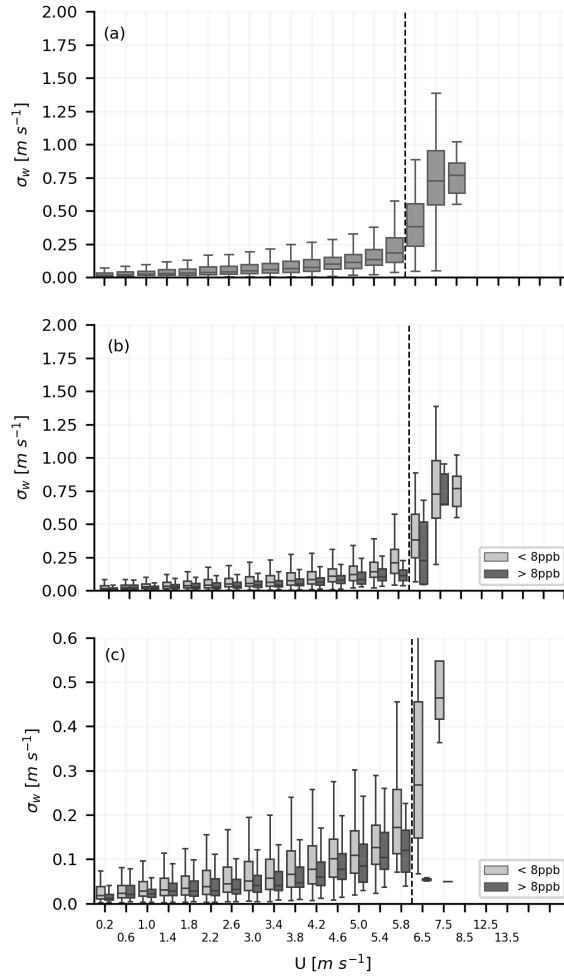
Figure 5: Same as Fig 10 in manuscript but using 5-minute averages.

[RC2.16]-P15,l4-11: This part looks more like methods, and not really results. Please define the Obukhov length L somewhere in the text.

[**AR2.16**] We have moved these lines to a new section in Methods. As explained in the following comment we have decided to not use the Obukhov length, therefore no definition is needed.

[RC2.17]-P15,l11-15: How the authors can explain nighttime unstable conditions above the canopy? I have seen some other studies reporting unstable conditions within closed canopy (even in Amazonia), but not above it, as one would expected large cooling on the top of the canopy.

[**AR2.17**] The referee is correct when indicating that the expected nighttime conditions above the canopy are stable. However, several studies have already shown that under certain conditions the stable layer above the Amazon canopy may break down (e.g. Fitzjarrald and Moore, 1990; Zeri and Sá 2011; Oliveira et al., 2018). One of the first works to report nighttime unstable conditions above

the Amazon canopy was Fitzjarrald and Moore (1990). According to them, there are cases when net radiative heat losses are sharply reduced at night, most likely because of increasing cloud cover. With reduced net radiation, there is eventually much-reduced cooling at canopy top to maintain the stable potential temperature. Recently Oliveira et al. (2018) also have shown that intermittent turbulence events, which are quite common in the Amazon NBL (frequently caused by the deep convection) can cause vertical exchange of scalars and have an effect on the local stability.

Furthermore, our interpretation of the results shown in Table 2 of the manuscript is the following. As we stated earlier, under very stable conditions submeso motions can still be relevant even at an averaging window of one minute. Under these situations and with weak wind speeds there is no turbulence, therefore the sensible heat flux can still be influenced by non-turbulent motions that can lead to negative values of L (with positive values of w'T', see Fig. 6-lower panel). In addition, the "very unstable" cases are also influenced by very small values of friction velocity (Fig. 6-middle panel). For the "moderately unstable" cases we see that at very rare occasions the potential temperature gradient is negative (see Fig 6-top panel). This can be explained by the advection of cold air, which leads to unstable conditions of the nocturnal boundary layer.

Considering how L can be affected and how using a "very unstable" regime classification for a study dealing with the stable boundary layer can lead to confusion, we have decided to use a different approach. Using the $\frac{d\theta}{dz}$ between 81 and 36 m will without doubt provide a cleaner assessment of stability. This is different than what is shown in Fig. 9 of the manuscript, because here we are using 1-minute data and taking into account the height difference. When separating between negative and positive values for $\frac{d\theta}{dz}$ we found that 99.95% of the above-8-ppb gradients are above zero. We have taken out Table 2 and added the following lines: More evidence about the dominant regime of the NBL when the positive gradients occur is given by the potential temperature gradient ($\frac{d\theta}{dz}$) between 81 m and 36 m. We found that 99.95% of the positive gradients occur with positive values of $\frac{d\theta}{dz}$.
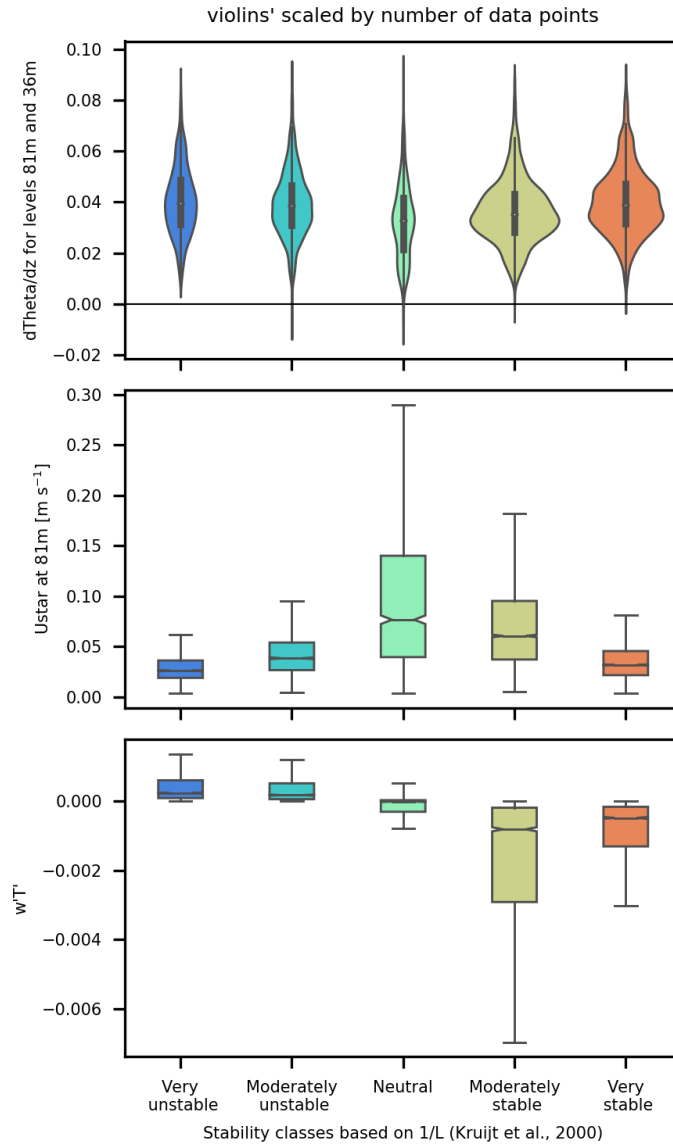
Figure 6: Potential temperature gradient violin plot showing the entire distribution of the data (top panel), friction velocity and w'T' box plots (middle and lower panel) for each of the stability classes defined in the manuscript based on Kruijt et al. (2000), Table 2 of the manuscript.

[**RC2.18**]-P19,l34: "....in this plot differs from that...."

    [**AR2.18**] Thanks for pointing this typo out. We have corrected it.

[**RC2.19**]-**Fig 4**: Why nighttime is defined including (probably for some seasons) sunset periods, but excluding sunrise hours? I understand that these atmospheric boundary layer transition periods are complicated, but they are also interesting. And are these criteria for separating nighttime and daytime holding for all seasons?

[**AR2.19**] We believe that the referee meant: Why nighttime is defined including (probably for some seasons) *sunrise* periods, but excluding *sunset* hours?. We have excluded sunset hours in the nighttime interval to avoid the afternoon transition period, in which the turbulent kinetic energy begins to decay rapidly within the boundary layer. This transition period influences the distribution and mixing of trace species, for example Vila-Guerau de Arellano et al. (2004) showed that during the afternoon transition chemical species emitted at the surface can rapidly reach the free troposphere. The onset of the positive gradient events studied here is, in most of the cases, late in the night as described in P6,l34-P7,l4, and are sustained until early morning. Therefore, by selecting this nighttime period we wanted to cover the full positive gradient episodes but without affecting early nighttime averages due to the afternoon transition. Thanks to the comment of the referee we realized that for Fig 4, we included 06:00 for both nighttime and daytime, using that data point in both populations. We have corrected this considering daytime hours from 07:00 to 18:00 and updated the figure. This subtle change did not lead to substantial differences in our results, only daytime percentages discussed in P6,l27-28, were slightly affected. In the revised manuscript these percentages are updated to the new values.

References:

Acevedo, O. C., Costa, F. D., Oliveira, P. E. S., Puhales, F. S., Degrazia, G. A., and Roberti, D. R.: The Influence of Submeso Processes on Stable Boundary Layer Similarity Relationships, Journal of the Atmospheric Sciences, 71, 207–225, https://doi.org/10.1175/JAS-D-13-50131.1, 2014.

Acevedo, O. C., Mahrt, L., Puhales, F. S., Costa, F. D., Medeiros, L. E., and Degrazia, G. A.: Contrasting structures between the decoupled and coupled states of the stable boundary layer: Stable Boundary Layer Coupling, Quarterly Journal of the Royal Meteorological Society, 142, 693–702, https://doi.org/10.1002/qj.2693, 2016.

Acevedo, O. C., Maroneze, R., Costa, F. D., Puhales, F. S., Degrazia, G. A., Martins, L. G. N., Oliveira, P. E. S., and Mortarini, L.: The Nocturnal Boundary Layer transition from Weakly to Very Stable. Part 1. Observations, Quaterly Journal of the Royal Meteorological Society, https://doi.org/10.1002/qj.3642, 2019.

Alekseychik, P., Mammarella, I., Launiainen, S., Rannik, Ü., Vesala, T.,: Evolution of the nocturnal decoupled layer in the pine forest canopy, Agricultural and Forest Meteorology, 174-175, 15-27, 2013.

Dias-Junior, C. Q., Sá, L. D., Marques Filho, E. P., Santana, R. A., Mauder, M., and Manzi, A. O.: Turbulence regimes in the stable boundary layer above and within the Amazon forest, Agricultural and Forest Meteorology, 233, 122–132, https://doi.org/10.1016/j.agrformet.2016.11.001, 2017.

Fitzjarrald, D. R. and Moore, K. E.: Mechanisms of nocturnal exchange between the rain forest and the atmosphere, Journal of Geophysical Research, 95, 16 839, https://doi.org/10.1029/JD095iD10p16839, 1990.

Kruijt, B., Malhi, Y., Lloyd, J., Nobre, A. D., Miranda, A. C., Pereira, M. G. P., Culf, A., and Grace, J.: Turbulence Statistics Above And Within Two Amazon Rain Forest Canopies, Boundary-Layer Meteorology, 94, 297–331, https://doi.org/10.1023/A:1002401829007, 2000.

Marht, L., Thomas, C., Richardson, S., Seaman, N., Stauffer, D., and Zeeman, M.: Non-stationary Generation of Weak Turbulence for Very Stable and Weak-Wind Conditions, Boundary Layer Meteorology, pp. 179–199, https://doi.org/10.1007/s10546-012-9782-x, 2013.

Mortarini, L., Cava, D., Giostra, U., Costa, F. D., Degrazia, G., Anfossi, D., and Acevedo, O.: Horizontal meandering as a distinctive feature of the Stable Boundary Layer. Journal of the Atmospheric Sciences, 76(10), 3029-3046, 2019.

Oliveira, P. E. S., Acevedo, O. C., Sörgel, M., Tsokankunku, A., Wolff, S., Araújo, A. C., Souza, R. A. F., Sá, M. O., Manzi, A. O., and Andreae, M. O.: Nighttime wind and scalar variability within and above an Amazonian canopy, Atmospheric Chemistry and Physics, 18, 3083–3099, https://doi.org/10.5194/acp-18-3083-2018, 2018.

Shuttleworth, W. J.: Daily variations of temperature and humidity within and above Amazonian forest, Weather, 40, 102–108,https://doi.org/10.1002/j.1477-8696.1985.tb07489.x, 1985.

Stefanello, M., Cava, D., Giostra, U., Acevedo, O., Degrazia, G., Anfossi, D., and Mortarini, L.:

Influence of submeso motions on scalar oscillations and surface energy balance. Quarterly Journal of the Royal Meteorological Society, 146(727), 889-903, 2020.

Stiperski, I., Calaf, M. and Rotach, M.W.: Scaling, anisotropy, and complexity in near-surface atmospheric turbulence. Journal of Geophysical Research: Atmospheres, 124, 1428–1448. https://doi.org/ 10.1029/2018JD029383, 2019.

Sun, J., Mahrt, L., Banta, R. M., and Pichugina, Y. L.: Turbulence Regimes and Turbulence Intermittency in the Stable Boundary Layer during CASES-99, Journal of the Atmospheric Sciences, 69, 338–351, https://doi.org/10.1175/JAS-D-11-082.1, 2012.

Vilá-Guerau de Arellano, J., Dosio, A., Vinuesa, J.-F., Holtslag, A. A. M., and Galmarini, S. The dispersion of chemically reactive species in the atmospheric boundary layer, Meteorol. Atmos. Phys., 87, 23–38, 2004.

Zeri, M., & Sá, L. D.: Horizontal and vertical turbulent fluxes forced by a gravity wave event in the nocturnal atmospheric surface layer over the Amazon forest. Boundary-layer meteorology, 138(3), 413-431, 2011.

Understanding nighttime methane signals at the Amazon Tall Tower Observatory (ATTO)

Santiago Botía B.[1], Christoph Gerbig[1], Julia Marshall[1], Jost V. Lavric[1], David Walter[1,2], Christopher Pölhker[2], Bruna Holanda[2], Gilberto Fisch[3], Alessandro Carioca de Araújo[4], Marta O. Sá[5], Paulo R. Teixeira[5], Angélica F. Resende[5], Cleo Q. Dias-Junior[6], Hella van Asperen[7], Pablo S. Oliveira[8], Michel Stefanello[8], and Otávio C. Acevedo[8]

[1]Max Planck Institute for Biogeochemistry, Hans-Knoell-Straße 10, 07745 Jena, Germany
[2]Max Planck Institute for Chemistry, 55020 Mainz, Germany
[3]Instituto de Aeronautica e Espaço (IAE), Departamento de Ciência e Tecnologia Aeroespacial (DCTA), São José dos Campos, SP, Brazil
[4]Empresa Brasileira de Pesquisa Agropecuária (EMBRAPA), Trav. Dr. Enéas Pinheiro, Belém, PA, Brazil
[5]Instituto Nacional de Pesquisas da Amazônia (INPA), Av. André Araújo 2936, Manaus, AM, Brazil
[6]Instituto Federal de Educação, Ciência e Tecnologia do Pará, Belém, PA, Brazil
[7]Institute of Environmental Physics, University of Bremen, Otto-Hahn-Alle 1, 28359, Bremen, Germany
[8]Departamento de Física, Universidade Federal de Santa Maria, Av. Roraima 1000, Santa Maria, RS, Brazil

Correspondence: Santiago Botía B. (sbotia@bgc-jena.mpg.de)

Abstract. Methane (CH_4) atmospheric mixing ratio measurements are analyzed for the period between June 2013 and November 2018 at the Amazon Tall Tower Observatory (ATTO). We describe the seasonal and diurnal patterns of nighttime events in which CH_4 mixing ratios at the uppermost (79 m a.g.l) inlet are significantly higher than the lowermost inlet (4 m a.g.l) by 8 ppb or more. These nighttime events were found to be associated with a wind direction originating from the southeast and wind speeds between 2 and 5 m s^{-1}. We found that these events happen under specific nighttime atmospheric conditions when compared to other nights, exhibiting less variable sensible heat flux, low net radiation and a strong thermal stratification above the canopy were found. Our analysis indicates that even at wind speeds of 5.8 m s^{-1} the turbulence intensity, given by the standard deviation of the vertical velocity, is suppressed to values lower than 0.3 m s^{-1}. Given these findings, we suggest that these nighttime CH_4 enhancements are advected from their source location by horizontal non-turbulent motions. The most likely source location is the Uatumã River, possibly influenced by dead stands of flooded forest trees that may be enhancing CH_4 emissions from those areas. Finally, biomass burning and the Amazon River were discarded as potential CH_4 sources.

1 Introduction

~~Atmospheric methane (CH_4) is, after carbon dioxide (CO_2), the most important anthropogenic greenhouse gas (Ciais et al., 2013)~~ .In the last decades atmospheric CH_4 has followed contrasting trends. Following decades of growth, during the period between 1999 to 2006, atmospheric CH_4 mixing ratios were stable (Dlugokencky E. et al., 2011), whereas during the last decade a steep growth has been reported (Nisbet et al., 2016). Currently the reasons for these trends are not clear and several explanations have been proposed (Nisbet et al., 2016; Schaefer et al., 2016; Turner et al., 2017; Rigby et al., 2017; Howarth, 2019). What

is evident in the current debate is that CH_4 emissions from tropical wetlands are the single largest source of uncertainty to the global CH_4 budget (Kirschke et al., 2013; Saunois et al., 2016). Recent estimates suggest that Amazon CH_4 emissions could contribute about a third of the global wetland CH_4 emissions (Pangala et al., 2017). Therefore, better knowledge of the seasonal and diurnal dynamics of these emissions will provide valuable insights for developing process-based models that

5 more accurately represent CH_4 emission and uptake (Turner et al., 2019). Our long term measurements of CH_4 mixing ratios at the Amazon Tall Tower Observatory (ATTO) provide an opportunity for better understanding such seasonal and diurnal dynamics, which are necessarily linked to atmospheric transport (Gloor et al., 2001).

CH_4 is transported from surface sources, which in the Amazon are dominated by wetland ecosystems (Saunois et al., 2016; Wilson et al., 2016), to the upper levels of the troposphere. Therefore, the vertical profile of CH_4 mixing ratios in the tropo-

10 sphere generally decreases with height, showing higher mixing ratios in the boundary layer (Miller et al., 2007; Beck et al., 2012; Webb et al., 2016). The profiles discussed in previous studies have been based on airborne measurements taken at daytime under well-mixed conditions during specific campaigns (e.g., Beck et al., 2012) or during regular sampling programs with aircraft flights at least twice per month (e.g., Gatti et al., 2014; Webb et al., 2016). These studies provide valuable insights about regional atmospheric transport (Miller et al., 2007), spatial distribution of dominant CH_4 sources (Wilson et al., 2016)

15 and the seasonal cycle across the Amazon region (Webb et al., 2016).

Closer to the surface, the proximity to the canopy and to the CH_4 sources becomes more important, dominating the variability of CH_4 mixing ratios at diurnal time scales. This strong variability is driven by a heterogeneous spatial distribution of sources (Gloor et al., 2001) and the complexity of atmospheric transport mechanisms in the first meters of the boundary layer (Stull, 1988). Despite these complexities, mixing ratio measurements close to the surface are the most feasible way to perform long-

20 term measurements at high temporal resolution that can provide insights at diurnal and seasonal time scales. However, such type of measurements are sparse in this region, particularly for CH_4.

There are two studies that provide an idea of the diurnal variability of CH_4 mixing ratios in the Amazon region (Carmo et al., 2006; Querino et al., 2011). Both of these studies were conducted in upland forest sites, similar to the present study. Carmo et al. (2006) performed CH_4 mixing ratios measurements during the dry and wet season at three different sites in the

25 Amazon. At all sites they focused their profile measurements on the canopy layer, which included one sampling inlet not more than 10 m above the canopy top. This study found that mixing ratios were generally higher at nighttime than during the day at all sites. As Carmo et al. (2006) focused on identifying local sources and calculating a local budget, the authors do not specify the amplitude of the diurnal cycle for the dry and wet seasons. Querino et al. (2011) provide one of the few records showing the diurnal variability of CH_4 above the canopy (53 m), as well as mixing ratio profiles within the canopy. CH_4 mixing ratios

30 above the forest were higher during the night than during the day. The amplitude of the diurnal cycle was particularly large in July (> 30 ppb), whereas in November there was no diurnal variability (Querino et al., 2011). Vertical CH_4 ~~profiles~~ mixing ratios inside the canopy were found to decrease with height, during both day and night, but more strongly during nighttime measurements, agreeing with Carmo et al. (2006). Both Querino et al. (2011) and Carmo et al. (2006) attributed this feature to a source located in the soil, and they both concluded that the upland forest is a source of CH_4. The observed high nighttime

CH$_4$ mixing ratios were explained by referring to a shallower nocturnal boundary layer that led to accumulation of CH$_4$ ÷above the canopy (at 53 m) in Querino et al. (2011) and throughout the canopy layer in Carmo et al. (2006).

In the present study we describe similar nighttime CH$_4$ mixing ratio patterns using the unprecedented long-term measurements at ATTO. This unique data set allows us to better describe the seasonal and diurnal variability of nighttime CH$_4$ signals at the 80 m tower. Furthermore, we provide a detailed analysis of the dominant atmospheric conditions under which high CH$_4$ mixing ratios are measured during the night at the top of the tower. Finally, we suggest possible sources of this nighttime CH$_4$ together with a description of the transport mechanisms that could be responsible for the vertical and horizontal transport of CH$_4$ in the nocturnal boundary layer.

2 Data and Methods

2.1 Site description

The Amazon Tall Tower Observatory (ATTO) research station was described in detail by Andreae et al. (2015); here we will only highlight aspects relevant to the current study. The ATTO site is located in the Uatumã Sustainable Development Reserve (USDR), which is 150 km northeast of the city of Manaus, in Central Amazonia. The site was built on a plateau (130 m-a.s.l) which is surrounded by a large drainage network composed of depressions or valleys at lower elevation, that which together with the plateaus form a small-scale heterogeneous topography with maximum height gradients of about 100 m (see Fig. 1).

The site is located in the interfluve between the Uatumã River and its tributary, the Abacate River. Both of these rivers flow in a NW to SE direction, merging their waters further southeast of the site. The flow of the Uatumã River is controlled by the Balbina reservoir, a hydroelectric dam located 55-60 km to the northwest of ATTO. The natural flood pulse of the Uatumã River was disturbed by the Balbina reservoir, causing large tree mortality along the riverside (Assahira et al., 2017; Resende et al., 2019). It is worth noting that the Abacate River has not suffered hydrological disturbances, still presenting a natural flooding seasonality.

The vegetation of the USDR is composed of different ecosystems. Upland dense forest (*terra firme*) is the characteristic vegetation on the plateaus and slopes, with the highest canopy when compared to the surrounding valleys (Andreae et al., 2015). The canopy height at ATTO is around 37 m, but the mean canopy height over the plateau is 20.7 ± 0.4 m (Andreae et al., 2015). In between the permanent flowing river channels and the *terra firme* forest, a savanna-type ecosystem on white-sand soil (*campina*) and forest on white-sand soil (*campinarana*) are found. In the *campina* there are smaller shrubs and trees with a vegetation height of 13.1 ± 2 m. The *campinarana* has a canopy with emergent trees up until 17 m (Klein and Piedade, 2019). Along the Uatumã and the Abacate rivers, seasonally flooded black-water forest (*igapó*) is the dominant type of vegetation (Andreae et al., 2015).

The regional atmospheric circulation has a seasonal pattern driven by the annual north-south shift of the Inter-tropical Convergence Zone (ITCZ) over the Atlantic Ocean (Andreae et al., 2012, 2015; Pöhlker et al., 2019). During the dry season, which we define here from July to October, ATTO is located south of the ITCZ. During the wet season, defined here from February to May, ATTO is located north of the ITCZ. This seasonal shift influences the origin of the air masses entering the

continent and arriving at ATTO. During the dry season the prevailing wind direction is from the east, whereas the wind direction during the wet season is predominantly from the northeast (Andreae et al., 2015). Easterly winds during the dry season transport air masses containing signals from biomass burning, occurring mainly in the eastern part of the arc of deforestation in Brazil. The northeasterly winds during the wet season are transported over a large fetch of continuous rainforest, yet containing high

5   background mixing ratios of greenhouse gases due to the influence of the northern hemisphere (Andreae et al., 2012, 2015). The dry and wet seasons were defined using precipitation data collected at the site with 30-minute resolution covering a period from January 2013 to December 2018. The highest precipitation values are recorded from February to May, with a maximum of 300 mm month^{-1} during March, while the lowest values, at below 100 mm month^{-1}, are found for the months between July and October (Fig. 2).

10   **2.2   CH$_4$ mixing ratio sampling system**

Our continuous measurements system was installed in March 2012 in the 80-m-tall tower. This tower was built during the pilot phase of an ongoing measurement program. There are five air inlets located at 79, 53, 38, 24 and 4 m above ground. At these heights, we measure atmospheric mixing ratios of CH$_4$, carbon dioxide (CO$_2$) and carbon monoxide (CO) using two Picarro Analyzers, the G1301 for CH$_4$ and CO$_2$ and the G1302 for CO$_2$ and CO. The G1301 analyzer (Serial CFADS-109)

15   provides data with a standard deviation of the raw data below 0.05 ppm for CO$_2$ and 0.5 ppb for CH$_4$. For the G1302 (Serial CKADS-018), the standard deviation of the raw data is 0.04 ppm for CO$_2$ and 7 ppb for CO. For more details on precision and long-term drift see Andreae et al. (2015). Similar to Winderlich et al. (2010), downstream of each sampling line 8 l stainless steel spheres act as buffer volumes. This buffer system provides ideal air mixing characteristics to have continuous near-concurrent measurements at all heights (Winderlich et al., 2010). In Winderlich et al. (2010) the buffers integrate the air

20   signal from every inlet with an e-folding time of approximately 37 min, with a flow of 150 standard cubic centimeter per minute (sccm), at 700 mbar. As we have two analyzers our time resolution is higher with an e-folding time of approximately 18 min (8 l/(150x2) sccm at 700 mbar). Therefore, we assume that the 15 min averages used in Sect. 3.2.3 correspond to independent samples. The standard data available at *http://attodata.org* are at 30-minute resolution.

2.3   Meteorological instrumentation

25   For this study we use wind direction, wind speed, air temperature, net radiation, precipitation and soil moisture. Sonic anemometers are fixed at 14, 22, 41, 55 and 81 m (above ground level; a.g.l.), but in this study we mainly use wind speed and direction at 81 m (Windmaster, Gill Instruments Limited). In Sect. 3.1 we show wind speed profiles for specific nights, ~~for these we use~~ using additional data from the sonic anemometers (model CSAT3, Campbell Scientific, Inc.) at 14, 41 and 55 m which perform fast response wind (u, v, and w) measurements. At 81 m molar densities of CO$_2$ and H$_2$O are measured with

30   an IRGA (LI-7500A, LI-COR Inc., USA). Air temperature is measured at 10 heights: 81, 73, 55, 40, 36, 26, 12, 4, 1.5 and 0.4 m (a.g.l) with a Termohygrometer (C215, ~~Rototronic~~ Rotronic Measurement Solutions, UK.). Net radiation is measured with a Net radiometer (NR-Lite2, Kipp and Zonen, Netherlands) at 75 m (a.g.l). For precipitation data, a rain gauge (TB4,

Hydrological Services Pty. Ltd., Australia) is installed at 81 m, and for soil moisture a water content reflectometer (CS615, Campbell Scientific Inc., USA) provides data for the depths: 0.1, 0.2, 0.3 0.4, 0.6 and 1 m.

2.4 Time period of data used

In the present study we have used CH_4 mixing ratio and meteorological data at different time resolutions. When mentioning meteorological data, we refer to the variables described in 2.3. To provide more clarity we specify what type of data were used in each section. In Sect. 3.2, 3.3.1 and 3.3.2 we used CH_4 mixing ratios and meteorological variables at 30-minute resolution. The CH_4 mixing ratio record covers the period from June 2013 to November 2018, which enabled us to study the diurnal and seasonal variability within this period. In Sect. 3.3.3, we used high-frequency (10 Hz) meteorological data, in particular all wind components (u, v and w), in order to associate turbulence regimes with CH_4 mixing ratios at 15-minute resolution. More on the assumptions to link high-frequency wind data with 15-minute mixing ratios is given ~~in Sect. 3.3.3.~~ below. In Sect. ~~4.1 we use CH4~~ 3.4, we use 30-minute averages of CH_4, CO and ~~black carbon~~ Black Carbon (BC) ~~concentrations, all at 30-minute, equivalent mass concentrations~~ to assess the influence of biomass burning emissions in our ~~CH4~~ CH_4 signals. The ~~BC data~~ raw BC mass concentrations at 1-minute time resolution were obtained using ~~the Multiangle~~ a Multi-angle Absorption Photometer (MAAP, model 5012, Thermo ~~Electron Group~~ Fisher Scientific, Waltham, USA), as described in ~~detail in Saturno et al. (2018)~~ ~~.~~ Saturno et al. (2018). The instrument measures the absorption coefficient of aerosol particles deposited on a filter, which is converted to BC mass concentration by assuming a mass absorption cross section of 6.6 m^2 g^{-1}. In Table 1, we provide a list of the data used in each section, specifying the time resolution and the period of time used.

2.5 CH_4 gradient definition

~~We have defined a~~ A CH_4 gradient ~~as the~~ is defined as CH_{4grad} = $CH_{4_{79m}}$ - $CH_{4_{4m}}$. We indicate that the units of the CH_{4grad} and the comparisons here are in parts per billion (ppb). We refer to a positive gradient when $CH_{4grad} > 0$ ppb, or to a negative gradient when $CH_{4grad} <$ ~~0.~~ 0 ppb. Note that positive gradients are related to higher CH_4 mixing ratios at 79 m than at 4 m, while negative gradients to higher mixing ratios at 4 m. Throughout this paper we also use a 8 ppb threshold for classifying positive gradients and negative gradients. In Sect 3.2 we use three classes. The first one refers to very strong positive gradients ($CH_{4grad} > 8$ ppb or above-8-ppb class); the second one to gradients in between -8 ppb and 8 ppb (-8 < CH_{4grad} < 8 ppb); the third one to very strong negative gradients ($CH_{4grad} < -8$ ppb). In Sect. 3.3, we have limited our analysis to two classes, $CH_{4grad} > 8$ ppb, and $CH_{4grad} < 8$ ppb (below-8-ppb class). The motivation to use 8 ppb as the threshold value is to leave out small mixing ratio variations and select very strong events. The $\pm$ 8 ppb threshold is conservative and filters for strong gradients, if we consider that the annual global increase in atmospheric CH_4 during the last three years was 7.06, 6.95 and 10.77 ppb yr^{-1} for 2016, 2017 and 2018 respectively (Dlugokencky and NOAA). It is always stated in the text which of these classes is being considered.

2.6   Analysis of 30-minute averages

3   ~~Results and Discussion~~

2.1   ~~Seasonal and diurnal patterns of CH_4 gradients at ATTO~~

~~In this section, we focus on~~ In Sect. 3.2, the ~~gradient between the~~ 30-min averages of CH4 mixing ratios were grouped into daytime and nighttime and further classified into the three classes as described in Sect. 2.5. In Sect. 3.3.1 strong CH_4 positive gradients were associated with wind direction by using the Openair package in R developed by Carslaw and Ropkins (2012). This R package provides useful predetermined functions to interpret air pollution characteristics based on wind speed, wind direction and other variables. Micro-meteorological data were used together with collocated CH_4 mixing ratio data at ATTO (Sect. 3.3.2). The heights of the highest sonic anemometer and the highest air inlet for CH_4 mixing ~~ratios measured at~~ ratio measurements differ by two meters, with the former at 81 m and the latter at 79 m ~~(above the canopy) and at 4 m (within the canopy). A strong positive gradient, when~~. We assume that the effect of the two meters can be neglected and thus interpret all the 81 m data as valid for 79 m. In order to maintain consistency, we used the same 8 ppb threshold as in Sect. 3.2, but this time we clustered the other two classes ($CH_{4_{grad}}$ ~~>~~ < -8 ppb and -8 < $CH_{4_{grad}}$ < 8 ppb~~)~~ into only one: below-8-ppb. The latter provides more clarity in the interpretation, as we are strictly interested in the above-8-ppb class.

2.7   Analysis of 1-minute averages

In Sect. 3.3.3 we analyze the CH_4 positive gradients for the stable boundary layer taking into account the turbulence regimes defined by Sun et al. (2012). For this analysis we use high-frequency data (10 Hz) for micro-meteorological variables but we averaged to 1-minute in order to be consistent with recent practice in nocturnal boundary layer studies (Marht et al., 2013; Acevedo et al., 2016, 2019) and to more strictly filter out low-frequency submeso fluctuations (i.e. non-turbulent motions at scales smaller than those at the mesoscale) (Mahrt, 2009) in all wind components. We focus on 6 months of 2014 (March, April, May, July, August and September). We have selected these months to target wet and dry seasons, and discarded June because it is considered a transition month based on precipitation. These turbulence regimes are classified into two classes: above-8-ppb and below-8-ppb. This classification is performed using the highest temporal resolution of CH_4 mixing ratio ~~at~~ data, which is 15 minutes. We assume that the gradient is constant for each 15-minute interval. For example, if the CH_4 gradient is 5 ppb at 21:00, we use the same value for every minute until 21:14.

3   Results

3.1   Example of CH_4 gradient events

In Fig. 3a we show a night in which a very strong positive gradient occurred. After 00:00 and before 01:00, there is a sudden and abrupt divergence of CH_4 mixing ratios measured at 79 m ~~is higher than at 4 m) could be associated with an air mass measured at~~. This increase in CH_4 is not seen at the first three measurement levels, while at 53 m is observed with some delay

and with less intensity. The divergence at 79 m reaches a CH_4 peak of 1960 ppb at around 04:00, at which point the lowest three inlets show CH_4 mixing ratios lower than 1880 ppb. At this time there is a strong thermal inversion for the air above the canopy and the wind speed at 81 m decreases to almost 1 m s^{-1}. The duration of this positive gradient, considering the time in which the 79 m ~~that is disconnected from the air~~ inlet had mixing ratios higher than 1880 ppb, was about 5 hours. These

5 positive gradient events are very common in our time series and they vary mainly in duration and magnitude. For the case shown in Fig. 3a, we can see that the decoupling between the air above and within the canopy ~~, resulting from atmospheric transport of *non-local* sources, with *non-local* referring to areas different from the plateau where the tower is located. For very strong negative gradients, when~~ was very strong up until 53 m. At the 53 m level the signal, first measured at 79 m, arrived about 30 minutes later when the CH_4 mixing ratio began to increase, but at the lower levels the behavior is completely

10 independent. Decoupled conditions can be explained by a very strong thermal inversion that obstructs vertical mixing, which could be triggered by wind shear under stable conditions (Mahrt, 2009).

For other cases in which we observed positive gradient events during nighttime, the signals measured at 79 m are then measured at the lowest inlet (4 m) after some time, varying from 30 minutes to 1.5 hours (see Fig. 3b). For these situations, when the coherent response at the lowest levels is within the next half an hour, it could be explained by the sequential sampling

15 (top-bottom) and the buffer volume in our measurement system. However, in the case of such a subsequent top-down signal we also find that the decoupling between the air above and within the canopy is weaker or non-existent.

The virtual potential temperature (Θ_v) profiles above the canopy at 22:00 and 02:00 show a very similar gradient with a weak thermal inversion. Interestingly, at 02:00 when the $CH_{4_{grad}}$ ~~< -8 ppb (i. e. CH_4~~ mixing ratio at 79 m ~~is lower than at 4 m~~ ~~), we assume they could be associated with local sources within the canopy. Later in Sect. 4.1 we discuss what are the potential~~

20 ~~*non-local* sources that might be driving the positive~~ reached the maximum, the wind speed at 81 m decreased to 1 m s^{-1} and for the same time the Θ_v profile showed a mild gradient of about 1.2 K. This mild temperature increase with height above 41 m indicates that the decoupling of the air above the forest is less strong, explaining why the CH_4 is measured subsequently at lower heights. Note that vertical transport for these situations is triggered by mechanical turbulence (generated by wind shear instabilities) or intermittent turbulence that, in the absence of a very strong thermal inversion, can transport CH_4 to the lower

25 inlets and inside the canopy (Oliveira et al., 2018). During this night, the gradient was less pronounced and it lasted for less time than in the night shown in Fig. 3a.

In Fig 3c a night in which no gradient was measured is shown. An almost constant Θ_v profile indicates the coupling of the air above the canopy for the three selected times of the night. The thermal gradient for the layer above the canopy is about 1.5 K. The CH_4 ~~gradients, hereafter simply referred to as~~ mixing ratios are very similar at all inlet heights for the full 24-hour

30 period. During this night the wind speed has both the largest values and the lowest variability during the course of the night. From these three cases, one can see that positive gradient events are associated with atmospheric stability and wind speed. However, as we show in the next section 3.3, the wind speed is not necessarily always weak for positive gradients.

3.2 Seasonal and diurnal patterns of CH_4 gradients at ATTO

In Fig. 4 we show ~~a monthly time series of the CH_4 gradient at ATTO. The data indicate~~ that for all years except 2016, monthly mean positive ~~gradients~~ CH_4 gradients (hereafter simply referred to as positive gradients) occur mainly during the dry season, whereas the mean gradient is close to zero during the wet season. The monthly mean gradient is significantly different from zero during the dry months, with p-values (two sided t-test) lower than 0.01. This positive gradient at ATTO is more pronounced during the month of August, when the lowest precipitation values are less than 50 mm (Fig. 2). A different behavior is observed for 2016, in which a strong negative gradient during June and July suggests a possible CH_4 source within the canopy measured at 4 m. The reason for this is unclear, yet we provide some ideas discussed later in this section. The dry season peak is also seen at the other measurement heights (not shown here), but at 79 m the measured CH_4 mixing ratios are the highest, indicating that non-local sources are predominant during this period of time.

It is interesting to note that in the dry season also the largest variability in the gradient was observed, as opposed to the reduced variability during the wet season and transition months such as December and January. ~~The difference in variability can be partly explained by the seasonal shift of the air masses arriving at ATTO, which was described in Sect.2.1. During the dry season, easterly winds transport strong signals of trace gases and aerosols associated with biomass burning activity in the southern and southeastern region of the Amazon basin (Andreae et al., 2015; Saturno et al., 2018). During the wet season relatively clean air arrives from the northeast, travelling along a very large fetch of rainforest (Andreae et al., 2015). However, as we will show in Sect. 3.4, biomass burning alone cannot explain the positive gradient events at ATTO.~~

The positive gradients observed during the dry season are associated with nighttime CH_4 mixing ratio peaks at 79 m. ~~When separating the measurements into daytime and nighttime, and grouping the half-hourly averaged gradients calculated from the measurements into three classes ($CH_{4grad} > 8$ ppb; $-8 < CH_{4grad} < 8$ ppb; $CH_{4grad} < -8$ ppb), one can estimate the fraction of time (separately for night and day) corresponding to each class. We hypothesize that the > 8 ppb class is the result of CH_4-rich air brought to ATTO and measured at 79 m, whereas the < -8 ppb class results from a nearby source within the canopy measured at 4 m.~~ Figure 5 depicts the fraction of time for daytime and nighttime measurements for each of the classes described ~~above.~~ in Sect. 2.6. For all months, daytime measurements (Fig. 5a) are within the -8 to 8 ppb range over 60% of the time. Gradients lower than -8 ppb or higher than 8 ppb are more frequent and increase their contribution to the total time during May, June, July, August and September. For these months negative gradients are measured ~~9%, 19%, 22~~8.7%, 18.6%, 22.3%, and ~~18% and 9~~17.6% and 7.8% of the total daytime hours, while positive gradients are found ~~5%, 7%, 12%, 14% and 10~~3.6%, 6.2%, 10%, 12.2% and 8.4%.

Nighttime measurements, in general, show a larger contribution of positive gradients to the total time (Fig. 5b). ~~Interestingly, nighttime~~ Nighttime positive gradients occur in all months of the year, from 4.1% of the time in January to ~~43~~43.3% of the time in August. The highest percentages are recorded during the dry season months of July (~~30~~30.2%), August (~~43~~43.3%) and September (~~30~~30.2%). Unsurprisingly, these months also have the highest mean nighttime gradients, with 2.6 ± 23 ppb, 9.7 ± 21 ppb and 6.2 ± 23 ppb for July, August and September, respectively. ~~Moreover, August has the highest nighttime median gradient (5.1 ppb), providing further evidence that positive gradients are more frequent during nighttime in this month.~~ The

8

maximum nighttime positive gradients were observed between 03:00 and 06:00 am local time (not shown), with values larger than 130 ppb. During daytime, the maximum positive gradients occur between ~~06~~07:00 and 08:00, with values over 150 ppb. Note that these gradients are generated during nighttime and can persist for a couple of hours until the erosion of the nocturnal boundary layer and subsequent growth of the convective boundary layer, which occurs between 08:00 and 09:00 am (local

5   time) (Fisch et al., 2004; Carneiro, 2018).

The mean diurnal cycles of the CH_4 gradient ~~measured between 79 m and 4 m (hereafter mean diurnal cycle gradient)~~ for dry and wet seasons provide interesting insights ~~.~~ (Fig. 6). The amplitude of the mean diurnal cycle gradient during the dry season (12.1 ppb) is 4 times larger than that of the wet season (2.7 ppb). This substantial difference can be attributed to two main reasons. First, due to strong nighttime positive gradients during the dry season, the maximum mean (7.1 ppb) is much

10   larger than the maximum mean of the wet season (0.5 ppb). Interestingly, both of these mean maxima occur at night, indicating that nighttime positive gradients are pulling up the mean in both seasons. Second, during the dry season the daytime planetary boundary layer is higher by a few hundred meters as a result of a larger sensible heat flux caused by the higher incoming shortwave radiation during this season (Fisch et al., 2004; Carneiro, 2018). ~~This~~ Under this case with higher mixing ratios close to the surface and lower free tropospheric mixing ratios (as shown for dry and wet seasons by Beck et al. (2012)), a

15   deeper boundary layer directly affects daytime CH_4 mixing ratios ~~,~~ because CH_4 ~~molecules~~ enhancements near the surface will be diluted in a larger volume~~, leading to lower CH_4 mixing ratios at 79 m~~. This dilution effect does not happen at the 4 m inlet, because the within-canopy air volume remains the same throughout the seasons. This boundary layer effect together with higher CH_4 mixing ratios at 4 m compared to 79 m during the dry season ~~yields~~ yield a lower dry season daytime mean minimum of -5.0 ppb, whereas the mean minimum during the wet season is -2.2 ppb.

20   Another possibility that might contribute to this seasonal difference is local production of CH_4 during the wet season. Though we lack long-term CH_4 flux measurements at the site, we can infer a potential local source during the wet season considering that the mean monthly gradient during daytime hours of the wet season is always negative (not shown), meaning that the CH_4 mixing ratio at 4 m is higher than at 79 m. Although outside of the scope of this study, strong negative gradients are more common during daytime, reaching differences as large as -455 ppb, measured in May of 2014. ~~In contrast, the largest~~

25   ~~negative nighttime gradient measured is -236 ppb, occurring in October of 2015.~~ The 4 m inlet is too high above the soil to ~~assume that this CH_4 signal comes directly from~~ directly associate this signal with the soil below, but is well within the canopy ~~,~~ indicating that the source must be local possibly within a horizontal distance of few hundred meters. The event in May 2014, coincided with a strong signal measured for carbon monoxide (CO) with the same timing, but not for carbon dioxide (CO_2), which suggests a source not related to combustion.

30   The mechanism producing this strong CH_4 signal within the canopy is currently under investigation, yet here we discuss what the potential sources could be. Our first thought ~~for the strong negative gradient during daytime~~ is that the soil on the plateau is producing CH_4 episodically. Given some additional parameters, we can calculate the water-filled pore space (WFPS) for the depth (60 cm) of maximum soil moisture content~~of~~, at which we believe CH_4 could be produced. To be conservative we take the mean soil moisture value for the entire record at 60 cm, 0.35 m^3 m^{-3}. ~~Based on Andreae et al. (2015) we know~~

35   ~~that~~ According to Andreae et al. (2015) 85% of the soil in the plateau is clay, ~~and thus~~ thus we use a soil particle density of

9

2.86 g cm^{-3} (Schjønning et al., 2017)). Also from Andreae et al. (2015), we use a bulk density of 1.1 g cm^{-3}. This results in a WFPS of 57% ~~which could~~, which is likely to enhance the abundance of anaerobic micro-sites where ~~CH$_4$ can be produced.~~ methanogenic bacteria can be activated. At values above 60% Verchot et al. (2000) found positive CH$_4$ fluxes, at the ATTO site values above 60% are often seen during the wet season. Upland *terra-firme* soils are generally considered as CH$_4$ sinks (Dörr

5   et al., 1993; Dutaur and Verchot, 2007; Saunois et al., 2016), but at local scales the soil can become a source depending on the balance between CH$_4$ production and oxidation (Verchot et al., 2000). Moreover, tree stems were found to play an important role as conduits for soil-generated CH$_4$ in upland *terra-firme* tropical forest (Welch et al., 2019). These findings, together with our data, suggest that the upland *terra-firme* CH$_4$ sink at ATTO ~~need~~ needs to be further studied.

A second option is related to daytime anabatic flows within the canopy transported from the depressions to the plateau (Tóta

10   et al., 2012). These anabatic flows could transport CH$_4$ produced in saturated soils of these low-lying areas. Recent (May 2019) unpublished CH$_4$ mixing ratio measurements suggest a possible source at the lowest point of one depression close to the ATTO site. A further possibility, not likely explaining the complete signal at 4 m, but probably contributing to it, might be termite production within the canopy. Termite CH$_4$ production is common in tropical ecosystems (Sanderson, 1996), however flux measurements from this source have not been performed at the site. The 2016 episode mentioned earlier provides evidence

15   that CH$_4$ mixing ratios at 4 m could be strongly enhanced by ~~unknown~~ unidentified processes that need further research. The natural variability of upland *terra-firme* CH$_4$ sources or sinks could have been altered by the El Niño event that began in 2015 and lasted until early 2016, as shown by Pfannerstill et al. (2018) for OH at the ATTO site. For these episodes, which occurred during June and July (see Fig. 4), the enhancement at 4 m lasted for more than 5 hours presenting the onset at nighttime and maintained during daytime. Furthermore, the air within the 4 m layer above the ground seemed to be strongly decoupled from

20   the layers above as none of the upper inlets measured the signal observed at 4 m (not shown). Therefore, the 4 m episodes described here are very likely a combination of an enhanced source and the stability conditions of the air within the canopy for those specific dates.

3.2.1   ~~Example of CH$_4$ gradient events~~

~~To give the reader an idea of how strong these nighttime positive gradients can be compared to nights with no gradient, three~~
25   ~~case studies are presented in Fig. 3. In addition to the CH$_4$ time series measured at different levels, profiles of virtual potential temperature and mean wind speed are shown to assess the air coupling above and within the canopy.~~

~~In Fig. 3a we show a night in which a very strong positive gradient occurred. CH$_4$ mixing ratios at all heights follow the same trend for the first hours of the night. From 19:00 to 00:00 there is a common increase of about 15 ppb at all heights. At 22:00 the Θ_v above the canopy shows a mild gradient with the canopy slightly cooler than the layers above. The Θ_v in the layer~~
30   ~~between 40 m and 80 m is constant, and the wind speed profile between the same heights changes by about 1 m s^{-1}. After 00:00 and before 01:00, there is a sudden and abrupt divergence of CH$_4$ mixing ratios measured at 79 m. This increase in CH$_4$ is not seen at the first three measurement levels, 4 m, 24 m and 38 m, while at 53 m is observed with some delay and with less intensity. The divergence at 79 m reaches a CH$_4$ peak of 1960 ppb at around 04:00, at which point the lowest three inlets show CH$_4$ mixing ratios lower than 1880 ppb. Note that at this time there is a strong thermal inversion for the air above the canopy~~

and the wind speed at 81 m decreases to almost 1 m s^{-1}. After sunrise, as the canopy and the first meters of the boundary layer are heated by incoming radiation, mixing ratios at all heights converge to the same behavior and show no significant differences. Note that the Θ_v profile at 08:00 decreases slightly with height and the wind speed has increased to more than 3 m s^{-1} at 81 m. The duration of this positive gradient, considering the time in which the 79 m inlet had mixing ratios higher than 1880 ppb, was about 5 hours. These positive gradient events are very common in our time series and, as we said before, are more frequent during August, but also occur in July and September. Positive gradient events vary mainly in their duration and the magnitude. For the case shown in Fig. 3a, we can see that the decoupling between the air above and within the canopy was very strong up until 53 m. At the 53 m level the signal, first measured at 79 m, arrived about 30 minutes later when the CH$_4$ mixing ratio began to increase, but at the lower levels the behavior is completely independent. The decoupling is due to a very strong thermal inversion that obstructs vertical mixing, which could be triggered by wind shear under stable conditions (Mahrt, 2009).

For other cases in which we observed positive gradient events during nighttime, the signals measured at 79 m are then measured at the lowest inlet (4 m) after some time, varying from 30 minutes to 1.5 hours (see Fig. 3b). For these situations, when the coherent response at the lowest levels is within the next half an hour, it could potentially be explained by the sequential sampling (top-bottom) and the buffer volume in our measurement system. However, in the case of such a subsequent top-down signal we also find that the decoupling between the air above and within the canopy is weaker or non-existent.

The Θ_v profiles above the canopy at 22:00 and 02:00 show a very similar gradient with a weak thermal inversion. Interestingly, at 02:00 when the CH$_4$ mixing ratio at 79 m reached the maximum, the wind speed at 81 m decreased to 1 m s^{-1} and for the same time the virtual potential temperature profile showed a mild gradient of about 1.2 K. This mild temperature increase with height above 41 m indicates that the decoupling of the air above the forest is less strong, explaining why the CH$_4$ is measured subsequently at lower heights. Note that vertical transport for these situations is triggered by mechanical turbulence (generated by wind shear instabilities) or intermittent turbulence that, in the absence of a very strong thermal inversion, can transport CH$_4$ to the lower inlets and inside the canopy (Oliveira et al., 2018). During this night, the gradient was less pronounced and it lasted for less time than in the night shown in Fig. 3a. At 07:30, CH$_4$ mixing ratios are very similar and the wind speed increase to more than 2.5 m s^{-1}.

In Fig 3c a night in which no gradient was measured is shown. For this night the coupling of the air above the canopy is shown by the almost constant Θ_v profiles for the three selected times of the night. The thermal gradient for the layer above the canopy is about 1.5 K. The CH$_4$ mixing ratios are very similar at all inlet heights for the full 24-hour period. During this night the wind speed has both the largest values and the lowest variability during the course of the night. From these three cases, one can see that positive gradient events are associated with atmospheric stability and wind speed. However, as we show in the next section, the wind speed is not necessarily always weak for positive gradients. Therefore, a deeper analysis of the main atmospheric conditions under which positive gradients are found is presented next.

3.3 Atmospheric characteristics of positive CH$_4$ gradients

As discussed in the previous section, a deeper understanding of the atmospheric conditions during positive gradient events is needed. In Sect. 3.3.1 and 3.3.2 the analysis is performed using 30-minute data for both CH_4 mixing ratios and micro-meteorological variables. In Sect. 3.3.3 we analyze the CH_4 positive gradients for the stable boundary layer taking into account the turbulence regimes defined by Sun et al. (2012). The stable boundary layer hereafter be referred to as the nocturnal boundary layer (NBL). These turbulence regimes were identified above another Amazon forest canopy by Dias-Junior et al. (2017) using 5-minute averages for wind speed and vertical velocity (w). Therefore in this analysis we use high-frequency data (10 Hz) for micro-meteorological variables but we averaged to 1-minute, in order to be consistent with recent practice in nocturnal boundary layer studies (Marht et al., 2013; Acevedo et al., 2016, 2019) and to more strictly filter out low-frequency submeso fluctuations (i.e. non-turbulent motions at scales smaller than those at the mesoscale) (Mahrt, 2009) in all wind components. CH_4 mixing ratios consist of 15-minute intervals because our sampling system is not designed for high-frequency measurements, this is the highest temporal resolution we can obtain. The way in which we associated the turbulent regimes with CH_4 positive gradients is explained below.

3.3.1 CH_4 positive gradients and wind direction for 2013-2018

Associating CH_4 positive gradients with the prevailing wind direction provides information about potential source areas. We have done this by using the Openair package in R developed by Carslaw and Ropkins (2012). This R package provides useful predetermined functions to interpret air pollution characteristics based on wind speed, wind direction and other variables. The analysis was performed at hourly and monthly time scales by calculating a mean $CH_{4_{grad}}$ for each bin conformed by wind direction and time of day (hourly) or wind direction and month (monthly), as shown in Fig 7. For hourly time scales, we find that for nighttime hours and when the mean $CH_{4_{grad}}$ is above 8 ppb the wind direction is within the range of 90 and 180 degrees, hereafter southeasterly (Fig. 7, left panel). Note that the wind directions ranging between 180-270 degrees, hereafter southwesterly, also show positive mean $CH_{4_{grad}}$ during nighttime hours but these are lower than those seen when the wind comes from the southeast. For lower or negative mean CH_4 gradients and other times of the day, mainly daytime, the wind direction does not show a dominant pattern.

At monthly time scales we observed similar behavior, with a dominant southeasterly wind direction for mean $CH_{4_{grad}}$ above 8 ppb and the dry season months of August and September. At this monthly time scale, during During August and September, the southwesterly direction shows mean $CH_{4_{grad}}$ above 4 ppb, suggesting that this wind direction plays an important role in the positive $CH_{4_{grad}}$ events. Yet, it is very clear that large positive $CH_{4_{grad}}$ are mainly driven by southeasterly winds. Given that there is a prevailing pattern at monthly and diurnal time scales we can suggest that the potential source of the nighttime positive CH_4 gradient is associated with this wind direction. During dry season months the wind is more frequently coming from the east whereas during the wet season there is a shift to northeasterly winds. *In-situ* measurements of wind direction confirm this pattern. The monthly mean wind roses (see Fig. A1) suggest show that the wind is more frequently coming from the east and it is more likely to bring air masses from the southeastern areas of ATTO during June, July, August and September. These months have wind direction frequencies close to 20% with wind speeds ranging from 1 to 7 m s^{-1}. The mean wind rose plots for each hour of the diurnal cycle (see Fig. A2) indicate that after 15:00 local time, wind directions in the 90-180

degrees quadrant become more important than in previous hours of the day, with frequencies of about 15%. After 18:00, the frequency increases at this wind direction until 23:00. These wind direction patterns together with the prevailing wind direction for the positive $CH_{4_{grad}}$ suggest that nighttime positive gradient are more frequent in the dry season due to the prevailing wind direction, being more likely to bring air masses from the potential source region located to the southeast of ATTO.

5 ~~More information about the location of the potential source is given by the dominant wind speed during the nighttime positive $CH_{4_{grad}}$. Keeping the conservative threshold value of 8 ppb used previously, which corresponds to the 88th percentile of the gradient ($CH_{4_{79m}}$ - $CH_{4_{4m}}$) distribution, we plotted the~~ The probability of measuring gradients above ~~this percentile~~ the 88th percentile (8 ppb) together with wind direction and wind speed at 81 m ~~(see~~ is shown in Fig. 8~~). From this we obtain some interesting information. First, the~~ . The highest probability (50%) of having a gradient above 8 ppb is associated with

10 a particular wind speed range, mainly from 4 to 5 m s^{-1}. This wind speed range is seen for different wind directions, with the two southern quadrants (from 90 to 270 degrees) having a very similar probability of 40 to 50%, with a slightly higher conditional probability in the southeastern quadrant than the southwestern quadrant. For the northwest quadrant (270 to 360 degrees) the probability observed is lower than 40% but interestingly the wind speed range holds. Therefore, the gradients above 8 ppb ~~, which are mainly occurring during nighttime, are~~ are associated not only with a range of wind directions but

15 also with a particular wind speed range. We showed previously that southeasterly winds are clearly bringing CH_4-enriched air masses, but there is also a 40% probability of having these enhancements (above 8 ppb) when the wind direction shifts to the southwesterly direction and also when it comes from the northwest with approximately 25% probability at wind speeds of 5 m s^{-1}. It is relevant to note that 68% of the positive $CH_{4_{grad}}$ occur at wind speeds ~~within the range of~~ between 2 ~~to~~ and 5 m s^{-1} (not shown), which in the southern quadrants still have a higher probability of occurrence~~higher than 20% and lower than

20 50%~~.

Considering these results, we can infer ~~the following about the source of the nighttime positive CH_4 gradients. First,~~ that dominant large scale circulation patterns explain why large positive CH_4 gradients are more common during the dry season months~~, and this is because~~ . Thus, the wind arriving at ATTO is more likely to come from the source areas to the south of the site. Moreover, this also explains why large positive CH_4 gradients are more strongly associated with the southeasterly

25 direction; wind direction frequency is larger for these months than for other months of the year. ~~Second, large~~ Large positive CH_4 gradients can also come from other wind directions, but they are less frequent~~because the wind is less likely coming from those directions~~. Therefore, we identify a potential source of the nighttime signals with a probability of 40% to 50% to the south of the ATTO site (see Fig. 8). Here it is important to recall that these percentages are based on the conservative threshold of 8 ppb, analyses not shown here using a lower threshold yield ~~a slightly higher probability. Third,~~ higher probabilities. The

30 nighttime average wind direction is more frequently coming from the southeast, explaining why positive $CH_{4_{grad}}$ are more strongly associated with these wind directions at this timescale.

3.3.2 Net radiation, sensible heat flux, friction velocity and thermal stratification for CH_4 positive gradients 2013-2018

~~In this section we assess the role of atmospheric stability on the nighttime positive CH$_4$ gradients. We used micro-meteorological data at 30-minute resolution collocated with the CH$_4$ mixing ratio data at ATTO, covering the time period between June 2013 and November 2018. The heights of the highest sonic anemometer and the highest air inlet for CH$_4$ mixing ratio measurements differ by two meters, with the former at 81 m and the latter at 79 m. We assume that the effect of the two meters can be~~

5 ~~neglected and thus interpret all the 81 m data as valid for 79 m.~~

~~To better understand the atmospheric characteristics under which nighttime CH$_4$ positive gradients occur, we use net radiation, sensible heat flux (H), friction velocity (u_*) and the virtual potential temperature (θ_v) together with the data points with a CH$_{4grad}$ above and below 8 ppb (see Fig. 9). The variability of these quantities is plotted for each hour of the night, beginning at 20:00 until 06:00 (local time). In order to maintain consistency, we used the same 8 ppb threshold as in Sect. 3.2,~~

10 ~~but this time we clustered the other two classes (CH$_{4grad}$ < -8 ppb and -8 < CH$_{4grad}$ < 8 ppb) into only one: below-8-ppb. The latter provides more clarity in the interpretation, as we are strictly interested in the above-8-ppb class.~~

Net radiation for the above-8-ppb class is more negative, indicating a stronger radiative cooling at ATTO (see Fig. 9a) when these episodes occur. Net radiation is less variable for positive gradients with lower mean and median values for all night hours. This ~~association~~ can be explained because positive gradients are more frequent during the dry season and in particular in

15 August, when there is less cloud cover, as can be inferred by our precipitation record (Fig. 2), and as reported in Andreae et al. (2015). Clear skies contribute with a more effective radiative cooling at the canopy top, leading to a stronger thermal inversion in the NBL. Net radiation estimates at ATTO provide indirect evidence that suggest a shallower NBL height during the dry season. ~~Net radiation values~~ Values above the canopy are more negative during the dry season than during the wet season (see Fig. B1), suggesting a strong thermal inversion driven by large nighttime radiative cooling at the top of the canopy. For ~~very~~

20 stable nights at the ATTO site, Oliveira et al. (2018) found that at 81 m the turbulent fluxes were clearly less variable than at lower heights, indicating a very shallow NBL height.

~~Positive CH$_4$ gradients are~~ The above-8-ppb class is associated with a less variable H (see Fig. 9b), tending to values close to zero. For ~~the above-8-ppb~~ this class, the mean and median values of H at the beginning of the night hours, mainly from 20:00 to 23:00, are slightly more negative than for the other class. After midnight these values tend to be closer to zero for the

25 above-8-ppb class, suggesting that the nocturnal boundary layer is more stable for positive gradient events. The variability of both classes between 20:00 and 23:00 is not as different as for the rest of the hours, but still is slightly lower for the above-8-ppb class. Considering the height at which the H is zero ~~,~~ a proxy to infer the NBL height, one could say that positive CH$_4$ gradient events are associated with a very shallow nocturnal boundary layer, close to 81 m. The seasonal difference in NBL height was studied by Carneiro (2018) during the GoAmazon campaign (Martin et al., 2016), using a ~~Ceilometer, a~~

30 ~~Lidar~~ ceilometer, a lidar and a SODAR, among other instruments. Carneiro (2018) found that the time to erode (total erosion is considered to be when sensible heat flux and net radiation become positive) the nocturnal boundary layer is larger during the wet season, suggesting a deeper NBL height as one of the reasons to explain this. It is worth noting that the ~~Ceilometer~~ ceilometer sensitivity differs between instruments and it can also be affected by changes in the background radiation (Wiegner and Geiß, 2012). The ceilometer used by Carneiro (2018) is a CL31 (Vaisala Inc., Finland) and the one at ATTO is a Jenoptik

35 CHM15kx, used recently by Dias-Júnior et al. (2019) to determine the mixing layer depth using only daytime backscatter

profiles. In another study with the Jenoptik CHM15kx, Wiegner and Geiß (2012) found that the lowest detectable mixing height is around 150 m, therefore nights with a NBL height lower than this might not be well captured. Furthermore, the study was conducted over pasture which has different roughness and radiative characteristics compared to old-growth forest, and as such the results cannot be extrapolated to ATTO. Nonetheless the study provides valuable information about seasonal

5   differences of the NBL height. ~~We assume that the estimates given by Carneiro (2018) show a realistic range of variability, as the study makes a thorough comparison between several instruments.~~

    ~~Additionally, positive gradients are~~

    Positive gradients are also associated with low friction velocity (u_*) variability as well as low mean and median values for all nighttime hours (see Fig. 9c). ~~The nighttime trend for u_* starts with similar mean and median quantities for both classes, above~~

10   ~~and below 8 ppb. At 21:00 and afterwards, positive gradients above 8 ppb show lower values and a more compact distribution.~~ As a measure of mechanical turbulence, low u_* values suggest that positive gradients occur mainly at low turbulence intensity. This finding is not surprising as strong stability and the absence of turbulence can lead to accumulation of trace gases in the NBL (Stull, 1988; Fitzjarrald and Moore, 1990) due to reduced vertical mixing. However, under this common assumption and considering that the NBL above the canopy can attain shallow depths, one would expect to measure the accumulation of trace

15   gases at least at the other inlet heights above the canopy or at inlet heights closer to the canopy, where the possible source could be located, but for many of ~~the positive gradients~~ these events this is not the case. The CH_4 signal that arrives at the uppermost inlet (79 m), driving a positive gradient, is often not seen at lower inlets. This is very often the case for the inlet at 38 m but less so for that at 53 m, indicating that the CH_4 rich air is advected within a layer that includes the 79 m inlet and sometimes the 53 m inlet, but not those below 53 m. Having low friction velocity values and considering that the dominant wind speeds at

20   which positive gradients have more probability of occurrence are between 2 to 5 m s^{-1} (see Fig. 8), suggest that CH_4 signals are transported mainly by horizontal non-turbulent motions, which are probably formed by inactive turbulence mainly seen at the upper layers. Such inactive turbulence contributes very little to the generation of turbulence as was indicated by Högström (1990). ~~Acevedo et al. (2016) showed that there is a wind speed threshold at a certain height, referred to as *crossover threshold*, at which the NBL switches from a vertically decoupled to a coupled regime. Using data from a 30 m tower, they found that for~~

25   ~~a wind speed close to 2 m s^{-1} (at 1 m), the 30-m layer was fully vertically coupled. Under decoupled conditions u_* increases with height and at each individual level this quantity is constant before the *crossover threshold*. Under a coupled NBL after the *crossover threshold*, u_* converges to similar values at all levels and increases with wind speed. Therefore, we believe that under positive gradients the NBL is strongly decoupled, with a layered profile of u_* until 80 m, but not necessarily with low wind speeds at this height.~~

30   ~~The apparent decoupling of the above-canopy air for positive gradients suggests a very strong thermal stratification below 79 m. The~~

    The difference of θ_v between 81 and 36 m is slightly higher for the above-8-ppb class than for the below-8-ppb class (see Fig. 9d). The difference between the median values of the two classes is approximately 0.5 K for all night hours, hinting at ~~a~~ relatively faster radiative cooling at the top of the canopy for the above-8-ppb class. The variability of this difference is very

35   similar between both classes, although the above-8-ppb class is more skewed towards positive values. The difference between

mean and median values for both classes is small, but the fact that we see a systematic difference at all night hours, strengthens the argument that thermal stratification is stronger when positive gradients occur than for the other class.

Recalling the aim of this section, i.e. to show general atmospheric characteristics for the positive gradient events, here we summarize the general characteristics of positive gradients:

5   1. The source region is south of ATTO. In particular the southeastern region has the highest probability (between 40-50%) of bringing air masses that result in positive gradients.

2. Positive gradients are associated with less variable H and possibly a lower NBL height.

3. Low u_* values indicate reduced mechanical turbulent motion and strong stability for positive gradient events.

4. Thermal stratification is stronger for positive gradient events, supporting the idea of a decoupled regime during these

10   events.

3.3.3   Association of positive CH$_4$ gradients and NBL turbulence regimes

In this section we proceed to assess the role of stability regimes in the positive gradient events. For this purpose, we focus on 6 months of 2014 (March, April, May, July, August and September). We have selected these months to focus purely on wet and dry seasons, and discarded June because it is considered a transition month based on precipitation. For these months we used

15   high-frequency (10 Hz) data at ATTO to define the turbulence regimes of the NBL based on Sun et al. (2012). These regimes are then classified into two classes, the same as we have described before: above 8 ppb and below 8 ppb. This classification is performed using the highest temporal resolution of CH$_4$ mixing ratio data, which is 15 minutes. We assumed that the gradient is constant for each 15-minute interval. For example, if the CH$_4$ gradient is 5 ppb at 21:00, we use the same value for every minute until 21:14. We have shown before in Sect. 2.2 that our CH$_4$ mixing ratio measurement system provides independent

20   samples for each inlet height about every 15 min.

As shown in Sect. 3.3.2, positive gradients occur under a decoupled regime, namely in the absence of full vertical connection within the tower layer above the canopy (Acevedo et al., 2016). Given these facts, the questions that arise with the information we have about the occurrence of positive gradients are 1. Are positive gradient events associated with a particular regime of the NBL? If so, 2. What can we infer about nocturnal transport mechanisms by which enhanced CH$_4$ signals are brought to the 79

25   m inlet using *in-situ* high-frequency micro-meteorological data?

To answer the first question, we We have defined the NBL turbulence regimes following the work of Sun et al. (2012), which was further applied by Dias-Junior et al. (2017) at another site within the Amazon forest. In regime 1, turbulence is produced by local shear at low wind speed and low σ_w. In regime 2, σ_w increases with wind speed and bulk shear in the NBL triggers turbulence (Sun et al., 2012). In Fig. 10a the standard deviation of the vertical velocity (σ_w) is plotted as a function of mean

30   horizontal wind speed (U) for all the data available in 2014 without differentiating between gradient classes. Here, one can see that the regime transition (between regime 1 and 2) occurs at the wind speed bin of 5.8 m s^{-1}, which comprises the range between 5.6 and 6.0 m s^{-1}. At this threshold the uppermost quartile of σ_w exceeds 0.5 m s^{-1} and the slope defined by median

16

values changes notably. Therefore, we define this bin as the wind speed threshold that marks the transition from regime 1 to regime 2. ~~In regime 1, turbulence is produced by local shear at low wind speed and low σ_w. In regime 2, σ_w increases with wind speed and bulk shear in the NBL triggers turbulence (Sun et al., 2012).~~ Subdividing this further into the gradient classes above and below 8 ppb (Fig. 10b), we observe that the variability of σ_w close to the wind speed threshold (bins 5.8 and 6.5

5   m s^{-1}) is reduced for the above-8-ppb class. The upper quartile of σ_w for the above-8-ppb class exceeds 0.5 m s^{-1} only up to 6.5 m s^{-1}. The median σ_w for both classes display a similar range of variability at 7.5 m s^{-1}. The above-8-ppb class has a different distribution in the same wind speed bins close to the wind speed threshold, having lower median values of σ_w. This finding implies that vertical motions are even more suppressed at 81 m for the above-8-ppb class, regardless of the wind speed exceeding the threshold value.

10   Given these facts, we can ~~answer the first question above, and~~ associate positive gradients with the more stable regime 1: low σ_w even at wind speeds exceeding the threshold value, identified without separating into gradient classes. In other words, the wind speed threshold under positive gradient events is shifted to a higher wind speed, maintaining low σ_w values. To account for wind speed variations that could affect our assumption of constant CH$_4$ mixing ratios for every 15-minute window, we have filtered out the 15-minute time periods in which the difference between the maximum and minimum wind speed is larger than

15   0.5 m s^{-1} (Fig. 10c). After filtering, the dependence of σ_w on wind speed shows a similar pattern for each of the classes. In general, σ_w is less variable for positive gradients events. However, the difference in wind speed threshold is even more evident at the wind speed bins of 5.9 and 6.1 m s^{-1}. ~~Conclusively, positive gradients are associated with the stronger stability of regime 1.~~ According to Sun et al. (2012), turbulence in regime 1 is weak and is controlled by vertical temperature gradients, in line with our finding of a stronger thermal stratification for positive gradients shown before. In regime 1 eddies generated at the

20   observation height triggered by local shear do not come into contact with the ground (Sun et al., 2012). This is because, as stated by Sun et al. (2012), the length scale of the local shear is smaller than the observation height.

More evidence about the dominant regime of the NBL when the positive gradients occur is given ~~in Table ??. The statistics are based on only nighttime data, namely a time period between 20:00 and 06:00 (local time). For the 1-minute data we used a record of 6 months in 2014, the same months as above. The values shown are affected by very large outliers, therefore for~~

25   ~~defining the minimum and maximum limits of the 1/L classes in Table ??, we rely on the upper and lower quartiles $\pm$ 1.5 * inter-quartile range (IQR) . In this way we are leaving some data points unclassified, which is why the percentages in Table ?? do not add up to 100% but still cover 77.1% of the positive gradient events during this period of time. Almost half of the positive gradient events, 49.1%, occur during moderately stable or very stable conditions, 6.7% under neutral conditions and 21.4% under moderately unstable and very unstable conditions. Having 49.1% of the nighttime episodes under moderately~~

30   ~~stable or very stable conditions is in line with the association with regime 1 in the turbulence regime analysis. The fact that 21.4~~ by the potential temperature gradient ($\frac{d\theta}{dz}$) between 81 m and 36 m. We found that 99.95% of the ~~events occur under moderately unstable or very unstable conditions indicates that a considerable portion of the positive gradient events can also occur even when vertical motions are present. These situations are very likely taking place when the wind direction coincides with that of the source location.~~

As shown before, half of the positive gradients occur under a moderately stable or very stable NBL, with low values of σ_w (even at relatively large horizontal wind speeds) and low u_* positive gradients occur with positive values of $\frac{d\theta}{dz}$. As a result, one can infer the absence of vertical motion driven by nighttime turbulent mixing motions at the tower location. We can only attribute this lack of vertical mixing above the canopy to the tower location. Therefore, we have to separate the NBL conditions at the tower and at the potential source location. Unfortunately, we only have measurements at the tower and it is not realistic to measure at all possible source locations. Thus, and elaborating further on the second question established above, the the transport mechanisms can be divided into 1. those responsible for vertical transport of CH_4 at the source location and 2. those responsible for the horizontal advection bringing the CH_4 signals to the tower. Nocturnal vertical exchange, the mechanisms referred to in 1., can be driven by intermittent turbulence (Acevedo et al., 2006; Oliveira et al., 2018), gravity waves (Fitzjarrald and Moore, 1990), katabatic or drainage flows (Goulden et al., 2006; Tóta et al., 2008; Araújo et al., 2008; Tóta et al., 20 and nocturnal land-river breezes (De Oliveira and Fitzjarrald, 1994; Sun et al., 1998). For the horizontal transport of More on the vertical and horizontal transport mechanisms is discussed in Sect. 4.2.

3.4 Rejecting biomass burning and the Amazon river as potential sources

The timing of the biomass burning season coincides with the dry season in the Amazon region (Gatti et al., 2014; van der Laan-Luijkx et al., , thus one could think that CH_4 from combustion is responsible for the positive gradients presented here. During incomplete combustion, CH_4 is co-emitted together with carbon monoxide (CO) (Akagi et al., 2011; Kirschke et al., 2013; Andreae, 2019) , thus CO is considered a good proxy for biomass burning and it can be used as a reference to get an idea of enhancement ratios due to fire emissions.

In Fig. 11 large CO mixing ratios (>200 ppb) are observed, suggesting that for these measurements we could have sampled air with biomass burning signals. However, these data points represent only 10% of the data shown. Moreover, biomass burning typically produces CH_4 in a certain emission ratio to CO, dependent on the fuel type (Andreae and Merlet, 2001; Andreae, 2019) . These reference ratios are shown as lines in Fig. 11 and it can be seen that very few points fall on the reference lines and the CH_4 mixing ratios are substantially enhanced compared to those of CO, indicating an additional source of CH_4 seen for all wind directions. The mean CO mixing ratio during nighttime in the dry season at 79 m (140 ± 1.6 ppb) is on average 33 ppb higher than during the wet season (107 ± 1.25 ppb), suggesting that during the dry season we observe a "background enhancement" of CO mixing ratios at ATTO. Therefore, we can conclude that CH_4 measurements at ATTO during the dry season will always have a contribution of biomass burning, but as Fig 11 shows this "background enhancement" of CO can not completely explain the additional CH_4 towards the tower, we have discarded a nocturnal low-level jet since these events are commonly associated with high of the positive gradients. Note that most of the data points are grouped below 200 ppb for CO, suggesting that positive gradients occur with CO mixing ratios close to the mean dry season mixing ratio. Given these facts, we believe that positive gradients have a minor contribution of CH_4 from biomass burning, but the magnitude of the CH_4 enhancement relative to the CO mixing ratios needs to have an additional source.

Therefore, the challenge constraining to what extent fire emissions affect our CH_4 relies on identifying a clear and distinctive fire plume that provides information on not only the CH_4:CO but also the ratio relative to other species. Considering that black

carbon (BC) particles are emitted in smoldering and flaming fires (Andreae and Merlet, 2001) together with CO and CH_4, we use BC measurements to gain more insights about the influence of fire emissions on the full CH_4 signal at ATTO. Following the same approach as in Fig 11, the BC:CO ratios in Fig 12 indicate a more clear fire signal for the ESE and SSE wind directions. Note that the time period used in this plot is five months shorter than in Fig 11 and contains fewer data points, yet some of those

5 points fall on the reference slopes of Andreae (2019). In general terms, even though fire signals are measured at ATTO during nighttime for positive CH_4 gradients as suggested by Fig 12, the nighttime CH_4 enhancements at 79 m are not fully explained by combustion. Most of the data points in the ESE wind direction match the reference slope for biofuel and tropical forest burning. Both linked to human activity and according to the comprehensive study of Pöhlker et al. (2019), in the ESE direction there is substantial fire activity, the rainforest has suffered more fragmentation and degradation and there are more settlements.

10 It is worth recalling that here we are focusing on nighttime data when stable atmospheric conditions prevail, therefore the BC associated with biofuel burning might come from nearby settlements. For other directions the fire signal is not so evident and for some data points the CO mixing ratio is very high. This can be seen for all wind directions, and we believe that this can be explained by a possible weakening of the BC:CO due to deposition of BC (Saturno et al., 2018). Last but not least, even though biomass burning takes place throughout the entire dry season, its influence at the ATTO site is more relevant during

15 October and November, as shown by Saturno et al. (2018) and our carbon monoxide time series. Despite being able to detect a clear fire signature, CH_4 enhancements are too high relative to CO suggesting that an additional source is needed to explain the positive CH_4 gradients enhancement during nighttime.

    The Amazon River was discarded as a potential source even though it coincides with the wind direction found for the positive gradients. The Amazon River is 120 km southeast of ATTO, which means that a strong CH_4 emission into the nocturnal

20 boundary layer will have to be advected at a wind speed of 6 m s^{-1} to reach ATTO in five hours. This might be possible on some occasions, but as we saw before (Fig. 8) positive gradients are associated with wind ~~speed, high friction velocities and weak to unstable conditions (Karipot et al., 2008), whereas positive gradients coincide with low u_* and a broad range of wind~~ speeds between 2 and 5 m s^{-1}~~, and they are not specifically associated with large wind speed . Therefore, we believe that horizontal transport of CH~~. Moreover, 80% of the wind speed for nighttime positive gradients is below 4 m s^{-1}. In addition,

25 we calculated the distance to the CH_4 ~~from the source location to the tower is driven by horizontal advection of the prevailing wind , bringing methane-rich air when the wind direction coincides with those~~ source by time-integrating the wind speed at 81 m from 20:00 (beginning of the night) until the first occurrence of a positive gradient (> 8 ppb). The distribution of these distances is shown in Fig. ~~7. More about these mechanisms will be discussed in the next section~~13. The distances with more counts are below 50 km, 90% of the data points fall below 100 km, and 80% of the data points are below 72 km. Given these

30 facts, the Amazon River is not considered as a potential source for the nighttime CH_4 positive gradients.

3.5 ~~Potential sources and transport mechanisms of positive nighttime CH$_4$ gradients~~

3.4.1 ~~Constraining the potential sources~~

4 Discussion

4.1 Constraining potential nighttime CH$_4$ sources

5   Based on the predominant wind direction of the positive gradients, we propose a potential source of the nighttime CH$_4$ signals
at the 79 m level. First in importance and most dominant is the southeastern quadrant, second in line is the southwestern
quadrant (see Fig. 7 and 8). In these directions lies the Uatumã River, which we believe is the ~~main and most likely~~ most likely
main source (but not unique) of the positive gradients seen at ATTO. In addition to the natural CH$_4$ production by this river,
~~we propose~~ there are two additional sources that could ~~add up to the natural production and~~ enhance CH$_4$ degassing from this
10 water body. The first one is related to an enhanced CH$_4$ concentration downstream of the Balbina reservoir. As it was shown
by Kemenes et al. (2007), the Balbina reservoir not only leaks methane at the turbine intake due to depressurization but it
also enhances CH$_4$ concentrations downstream along the Uatumã river. Kemenes et al. (2007) found that CH$_4$ concentrations
in the Uatumã River decreased gradually until 30 km below the Balbina reservoir and remained constant for the next 70
km. It is worth noting that the CH$_4$ concentrations in the river ~~, reported by Kemenes et al. (2007),~~ were on average 24 μM
15 (Kemenes et al., 2007), three orders of magnitude higher than the average background value (0.05 μM) for Amazonian rivers
(Richey et al., 1988; Kemenes et al., 2007). The second additional source is very likely decomposition of dead flooded forest
stands downstream the Balbina reservoir along the Uatumã River. The dead stands are a consequence of the Balbina damming,
which has changed the natural flooding pulse along the river, causing massive mortality of flooded forest trees along a 80 km
stretch downstream of the dam (Resende et al., 2019). These dead stands were mapped recently by Resende et al. (2019), and
20 their spatial distribution coincides with the wind directions associated with the positive gradient events (see Fig. C1).

~~Here we suggest the Uatumã River as the dominant source of nighttime~~ Rivers also emit carbon dioxide (CO$_2$), but the CH$_4$
~~positive gradients, but we want to make clear that~~ enhancements described here do not coincide with an increase of CO$_2$. This
is mainly because nighttime respiration is very strong and any non-local enhancement at 79 m is masked by local CO$_2$ signals
at lower levels.

25 In addition, CH$_4$ could also be produced in the topographic depressions or valleys that form the drainage network surround-
ing ATTO. We have mentioned earlier that unpublished measurements of atmospheric CH$_4$ mixing ratios performed recently
in one of these valleys indicate a nighttime increase of CH$_4$ within the canopy. Based on Junk et al. (2011), these depressions
can be classified as *wetlands subjected to unpredictable, polymodal flood pulses fed by rainwater*, with low nutrient availability
compared to the plateaus. The flooding dynamics are driven by flash flood pulses after precipitation events, which can flush out
30 a large amount of the organic material available for decomposition (Wittmann F., 2019, personal communication). Therefore,
these depressions were assumed to have low potential of producing CH$_4$. Nevertheless, the accumulation seen for CH$_4$ mixing
ratio measurements performed during May and June in 2019 indicate that either CH$_4$ is transported to the lowest part of the

valley and accumulates during the night, or that CH_4 is produced at the valley and accumulated *in-situ*. ~~Therefore, we suggest two potential CH_4 sources. First, the Uatumã River and the downstream dead stands as the most likely one and second, the valleys in the ATTO surroundings.~~

The question that arises here is, why do we see a seasonal pattern in the positive gradients, being more frequent and pre-
5 dominant during the dry season? Considering the Uatumã River as the main source, we can explain this seasonality based on the effectiveness with which methane is degassed from the river to the atmosphere and the prevailing atmospheric conditions that drive atmospheric transport from the river to ATTO. During the dry season, when the river levels are low, degassing is more effective due to lower hydrostatic pressure, rendering the ebullitive pathway more efficient due to a shorter water column, which also reduces the probability of oxidation (Sawakuchi et al., 2014).

10 Therefore, during the dry season the CH_4 produced in the river sediment plus that added by the Balbina reservoir could be more effectively emitted to the atmosphere. It is important to note here that the suggested source coming from the anaerobic decomposition of the dead stands of flooded forests or *igapós*, could also be affected by the shorter water column during the dry season. However, in terms of enabling anaerobic conditions in the sediments, we have to make a distinction between floodplain and riverine environments, as these could have different responses to flooding. Anaerobic conditions in floodplains soils seem
15 to follow the established idea that with a higher water level there should be higher methane emissions (Kaplan, 2002; Bloom et al., 2012; Melton et al., 2013; Ringeval et al., 2014; Bloom et al., 2017), which are either diffused or transported by ebullition or trees (Pangala et al., 2017) to the atmosphere. In contrast, sediment in rivers could always be anaerobic with the potential to produce methane regardless of the season. What is really affected by a deeper water column in a river is the time for CH_4 to be oxidized and the increased hydrostatic pressure that can inhibit the ebullitive pathway (Sawakuchi et al., 2014).

20 Given the aforementioned, we can now link these potential sources along the Uatumã river and its seasonal pattern with the dominant atmospheric conditions during the dry season months. During these months and in particular in August ~~, as we have shown in the last section, the~~ the frequency with which the wind brings air from the southeast to ATTO is higher than during the wet season months, when the prevailing wind direction is ~~due~~ from the northeast (see Fig. A1). Therefore, the probability of advecting methane-rich air emitted in the Uatumã River area and potentially the valleys along that same direction is also
25 higher during the dry season.

~~The Amazon River was discarded as a potential source even though it coincides with the wind direction found for the positive gradients. The Amazon River is 120 km southeast of ATTO, which means that a strong CH_4 emission into the nocturnal boundary layer will have to be advected at a wind speed of 6 m s^{-1} to reach ATTO in five hours. This might be possible on some occasions, but as we saw before (Fig. 8) positive gradients are associated with wind speeds between 2 and 5 m s^{-1}.~~
30 ~~Moreover, 80% of the wind speed for nighttime positive gradients is below 4 m s^{-1}. In addition, we calculated the distance to the CH_4 source by time-integrating the wind speed at 81 m from 20:00 (beginning of the night) until the first occurrence of a positive gradient (> 8 ppb). The distribution of these distances is shown in Fig. 13. The distances with more counts are below 50 km, 90% of the data points fall below 100 km, and 80% of the data points are below 72 km. Given these facts, the Amazon River is not considered as a potential source for the nighttime CH_4 positive gradients.~~

4.1.1 ~~Atmospheric transport mechanisms from the source~~

4.2 Atmospheric transport mechanisms from the source

~~We have linked the seasonal pattern seen for the positive gradients to the location of the CH$_4$ sources and the driving atmospheric conditions responsible for horizontal transport. Now we proceed to describe in more detail the mechanisms by~~
~~which CH$_4$ is transported vertically at the source location. As we lack *in-situ* measurements at the proposed source locations, we build upon previous studies that have discussed mechanisms of vertical exchange of scalars in the NBL and assume that methane-rich air is transported vertically, from the surface to the upper layers of the NBL, by these mechanisms at the source location. Earlier in Sect 3.2.3, we listed some of these mechanisms, here we will address them while taking into account their probability of occurrence at the Uatumã River and at the valleys surrounding the tower~~ Nocturnal vertical exchange, can be driven by intermittent turbulence (Acevedo et al., 2006; Oliveira et al., 2018), gravity waves (Zeri and Sá, 2011), katabatic or drainage flows (Goulden et al., 2006; Tóta et al., 2008; Araújo et al., 2008; Tóta et al., 2012) and nocturnal land-river breezes (De Oliveira and Fitzjarrald, 1994; Sun et al., 1998). Intermittent turbulence mainly occurs as top-down bursts (Sun et al., 2012) that can connect the upper layers of the NBL with the canopy and even penetrate the upper part of it, as was shown to be important for ozone and CO$_2$ fluxes at the ATTO site by Oliveira et al. (2018). However, as intermittent turbulence (or regime 3 events as defined by Sun et al. (2012)) are mainly observed as top-down intrusions, we discard it as a vertical transport mechanism at the source locations ~~,~~ given that the source of CH$_4$ has to be at the surface. Gravity waves were shown to be responsible for transporting mass out of the sub-canopy layer during strong stability conditions and clear nights (Fitzjarrald and Moore, 1990), yet Cava et al. (2004) suggested that wave motions do not play an important role in scalar transport over a pine forest, based on the fact that one wave period had zero mean flux. Furthermore, Zeri and Sá (2011) for a study in based in the Amazon, found that the wave passage was not directly associated with vertical fluxes of CO$_2$. Therefore, it is difficult to firmly associate gravity waves with a vertical transport of CH$_4$ at the valleys or at the Uatumã River.

Having discarded these mechanisms, we believe that land breezes and drainage flows are the most probable ~~mechanisms~~ inducing vertical transport at the Uatumã River and ~~at~~ the valleys close to ATTO. During the night, due to differential radiative cooling over land and water, the river is warmer than the forest, leading to slightly warmer air over the water. This leads to a breeze from the land to the water that can transport ~~water vapor and~~ trace gases from the forest to the river. Such breeze (from land to water) was observed over the Balbina reservoir by Vale et al. (2018), finding a nocturnal accumulation of CO$_2$ over the water. Measurements during the ABLE experiment showed that the Amazon River could be 6 degrees warmer than the forest (De Oliveira and Fitzjarrald, 1994). Considering that black water rivers, such as the Uatumã are warmer than white water rivers, like the Amazon River, it is very likely that the Uatumã River is warmer than the surrounding forest. The temperature difference produces a pressure gradient as warm and less dense air moves vertically over the river. These air parcels can vertically transport CH$_4$ to upper ~~layer~~ parts of the NBL. This mechanism was described as a "chimney effect" in the study of Sun et al. (1998), in which they found that water vapor, ozone and CO$_2$ can be vertically transported by these events over a lake. The width of the lake in their study was about 10 km, and the width of the largest open water flooded areas along the Uatumã River southeast of ATTO, the Lago Cumateúba and Lago Araçatuba, are 3.5 km and 1.8 km.

The vertical transport mechanism at the valleys could be slightly different from that over the river. We believe that updrafts driven by air convergence forced by drainage flows can lead to vertical transport. Drainage flows in the Amazon were inferred by Goulden et al. (2006) using *in-situ* measurements and remote sensing imagery and although vertical transport mechanisms at the lower topographic areas were not addressed, they suggest that the air at the center could be well-mixed. Later, Araújo

5   et al. (2008) showed that nocturnal katabatic flow from the plateau to the valley not only affects the horizontal distribution of CO_2 mixing ratios along a topographic gradient but also the vertical profile of CO_2 mixing ratios over the valley. They had tower measurements on the plateau, on the slope and at the valley floor. With this setup they could confirm the occurrence of a shallow convergence zone over the valley that breaks down the thermal inversion and transports air vertically from the valley floor to the layers above. Araújo et al. (2008) suggest that the air might sink over the slope to maintain the local

10   circulation, but the katabatic or drainage flow at ATTO could be more pronounced due to steeper slopes compared to those in ~~the Araújo et al. (2008)study~~Araújo et al. (2008). On a different study ~~in the Amazon forest~~ (Tóta et al., 2012), drainage flows were found to occur above the canopy, moving from the plateau to the valley as in Araújo et al. (2008), but in the sub-canopy layer they observed upward (anabatic) flow during nighttime. If this process occurs at the ATTO site despite its steeper topographic gradients, it would not explain the observed positive CH_4 gradients. Such a mechanism would instead result in

15   negative CH_4 gradients as the CH_4 signal would arrive first to the 4 m inlet~~, which is not the case for positive gradients~~.

~~Due to the lack of measurements at the valley, we are limited to the studies we have cited previously and it is difficult to identify a dominant mechanism for vertical transport at these sites. However, we suggest the Uatumã River as the most likely CH_4 source area, with possible contributions from the valleys surrounding ATTO. In the next section we discuss why biomass burning does not explain the positive gradients even though the timing suggests it.~~

20   **4.2.1   ~~Rejecting biomass burning influence on positive CH_4 gradients~~**

~~The timing of the biomass burning season coincides with the dry season in the Amazon region (Gatti et al., 2014; van der Laan-Luijkx et al., , thus one could think that CH_4 from combustion is responsible for the positive gradients presented here. During biomass burning, in particular in the case of incomplete combustion, CH_4 is co-emitted together with carbon monoxide (CO), amongst other gases and particles (Akagi et al., 2011; Kirschke et al., 2013; Andreae, 2019). Because CO is emitted in large quantities~~

25   ~~and due to its low background mixing ratio, this species is considered a good proxy for biomass burning and it can be used as a reference to get an idea of enhancement ratios due to fire emissions. Figure 11 presents a scatter plot of the 30-minute~~ For the horizontal transport of ~~CH₄ and CO mixing ratios for nighttime measurements (at 79 m) during which a positive gradient was observed and the wind was coming from the southern quadrants. Here, we observed large CO mixing ratios (>200 ppb), suggesting that for these measurements we could have sampled air with biomass burning signals. However, these data points~~

30   ~~represent only 10% of the data shown. Moreover, biomass burning typically produces CH_4 in a certain emission ratio to CO, dependent on the fuel type Andreae and Merlet (2001); Andreae (2019). These reference ratios are plotted as slopes in Fig. 11 and it can be seen that very few points that fall on the reference slopes and the CH_4 mixing ratios are substantially enhanced compared to those of CO, indicating an additional source of CH_4 seen for all wind direction. The mean CO mixing ratio during nighttime in the dry season at 79 m (140 ± 1.6 ppb) is on average 33 ppb higher than during the wet season (107 ± 1.25 ppb),~~

suggesting that during the dry season we observe a "background enhancement" of CO mixing ratios at ATTO. towards the tower from the source location, we have discarded a nocturnal low-level jet since these events are commonly associated with high wind speed, high friction velocities and weak to unstable conditions (Karipot et al., 2008), whereas positive gradients coincide with low u_* and a broad range of wind speeds between 2 and 5 m s^{-1}, and they are not specifically associated with

5   large wind speed. Therefore, we can conclude that CH$_4$ measurements at ATTO during the dry season will always have a contribution of biomass burning, but as Fig 11 shows this "background enhancement" of CO can not completely explain the additional CH$_4$ of the positive gradients. Note that most of the data points are grouped below 200 ppb for CO, suggesting that positive gradients occur at CO mixing ratios close to the mean dry season mixing ratio. Given these facts, we believe that positive gradients have a minor contribution believe that horizontal transport of CH$_4$ from biomass burning, but the magnitude

10   of the CH$_4$ enhancement relative to the CO mixing ratios needs to have an additional source . the source location to the tower is driven by horizontal advection of the prevailing wind, bringing methane-rich air when the wind direction coincides with those shown in Fig. 7.

Therefore, the challenge constraining to what extent fire emissions affect our CH$_4$ relies on identifying a clear and distinctive fire plume that provides information on not only the CH$_4$:CO but also the ratio relative to other species. Considering that black

15   carbon (BC) particles are emitted in smoldering and flaming fires (Andreae and Merlet, 2001) together with CO and CH$_4$, we use BC measurements to gain more insights about the influence of fire emissions on the full CH$_4$ signal at ATTO. Following the same approach as in Fig 11, the BC:CO in Fig 12 suggests a more clear fire signal for the ESE and SSE winddirections. Note that the time period used in this plot differs form that in Fig 11 and contains fewer data points, yet some of those points fall on the reference slopes of Andreae (2019). In general terms, even though fire signals are measured at ATTO during nighttime

20   for positive CH$_4$ gradients as suggested by Fig 12, the nighttime CH$_4$ enhancements at 79 m are not fully explained by combustion. Most of the data points in the ESE wind direction match the reference slope for biofuel burning, which is defined by Akagi et al. (2011) as *biomass used as a domestic or industrial energy source*. Hence, biofuel burning is associated with human activity and according to the comprehensive study of Pöhlker et al. (2019), in the ESE direction there is substantial fire activity, the rainforest has suffered more fragmentation and degradation and there are more settlements. It is worth recalling that

25   here we are focusing on nighttime data when stable atmospheric conditions prevail, therefore the BC associated with biofuel burning might come from nearby settlements. For other directions the fire signal is not so evident and for some data points the CO mixing ratio is very high. This can be seen for all wind directions, and we believe that this can be explained by a possible weakening of the BC:CO due to deposition of BC (Saturno et al., 2018). In summary, despite being able to detect a clear fire signature, CH$_4$ enhancements are too high relative to CO suggesting that an additional source is needed to explain the positive

30   CH$_4$ gradients enhancement during nighttime.

5   Conclusions

In this paper we have studied CH$_4$ mixing ratios measured at ATTO. We showed that during the dry season, CH$_4$ mixing ratios are on average higher at the top of the 80 m tower than at the lower inlet heights. We have defined these events as positive

CH$_4$ gradients based on the condition: CH$_{4_{79m}}$ - CH$_{4_{4m}}$ > 8 ppb, which was applied to 6 years of continuous measurements at 30-minute resolution to classify our measurements. The CH$_4$ positive gradients of the dry season are associated with very strong CH$_4$ signals measured at 79 m, that occur more frequently during nighttime. Nighttime positive gradients (CH$_{4_{79m}}$ > CH$_{4_{4m}}$) are more frequent during July, August and September, occurring 43% of the time during nights in August, the month with the highest mean nighttime gradient (9.7 ± 21 ppb). At the diurnal time scale, we found that the . The amplitude of the mean diurnal cycle of the CH$_4$ gradient during the dry season is four times larger than that of the wet season due to the strong nighttime positive gradients. The dominant wind direction for these nighttime episodes, at monthly and diurnal time scales, is southeast of ATTO. In addition, this direction has the highest probability, 50%, of bringing air that will cause a positive gradient (> 8 ppb). This probability was also found to be linked to a wind speed range between 4 and 5 m s^{-1}. This wind speed was associated with positive gradients for other wind directions as well, but with a lower probability. The dominant atmospheric conditions under which positive gradients occur are moderately and very stable conditions. When comparing the gradient data classes of > 8 ppb and < 8 ppb, we found that the first class can be described as having lower despite these moderate wind speeds, these CH$_4$ enhancements showed lower net radiation (it is more negative by -2 to -3 W m^{-2}, see Fig. 9), less variable sensible heat flux, low friction velocity (< 0.3 m s^{-1}) and a strong thermal inversion above the canopy. Further analysis of high-frequency micro-meteorological data suggests that positive gradients are associated with regime 1 of the nocturnal boundary layer, in which turbulence is weak, controlled by temperature gradients and generated by wind shear (Sun et al., 2012).

We discarded Based on CH4:CO enhancement ratios, we excluded biomass burning as the main driver of the positive gradients, and have shown that the Uatumã River is very likely the most important source, due to the coincidence with the dominant wind direction. In addition, we suggest that two additional CH$_4$ sources might enhance the natural emissions from the river area. The first one is a Balbina-reservoir-driven increase in CH$_4$ concentrations in the river (Kemenes et al., 2007), and the second possible source of CH$_4$ is due to anaerobic decomposition of dead stands of flooded forest along the Uatumã River downstream of the reservoir (Resende et al., 2019).(i.e. the areas mapped by Resende et al. (2019)).

The atmospheric transport mechanisms were divided into those responsible for horizontal advection of CH$_4$ from the source locations to the ATTO site, and those that transport air vertically from the source location to the upper layers of the nocturnal boundary layer. We suggest that vertical transport over the Uatumã River results from differential radiative cooling of the forest and the water, producing a horizontal pressure difference that causes an upward displacement of air parcels over the river and transporting CH$_4$ aloft. These air parcels are then advected by the prevailing horizontal wind towards the ATTO site and subsequently measured at the 79 m level.

In the near future the 325 m tower will be fully equipped, providing valuable information in terms of CH$_4$ mixing ratios and meteorological variables which will enable us to study if the positive gradient extends to upper layers of the nocturnal boundary layer. We will be able to assess the influence of the residual layer and the height of the nocturnal boundary layer in our CH$_4$ measurements. To better understand local circulation and its effect on vertical CH$_4$ transport, we strongly recommend performing profile measurements at the river and in nearby valleys with emerging measurement techniques, such as unmanned aerial vehicles. High resolution atmospheric transport models, such as the Weather Research Forecast for greenhouse gases (WRF-GHG), could also help to understand and either reject or confirm the mechanisms mentioned here. Furthermore, an

upcoming campaign at ATTO specifically aims to determine the isotopic signature of the CH_4 mixing ratio during a positive gradient event, providing more accurate information about the CH_4 source.

Author contributions. SBB and CG designed the study and wrote the manuscript with assistance of JM, GF and HvA. JL and DW maintain the greenhouse gas measurement system at ATTO and provided the CH_4 data. ACA, MOS, PRT operate and maintain the micrometeorology equipment at ATTO and provided the data which was fundamental for this study. AFR provided the flooded forest dead stands data. CQDJ, PSO, MS and OCA contributed with the analysis and discussion of Sections 3.2 and 3.3. All co-authors contributed to the final manuscript.

Competing interests. The authors declare that they have no conflict of interest.

Disclaimer. Special issue statement. This article is part of the special issue "Amazon Tall Tower Observatory (ATTO) Special Issue".

References

Acevedo, O. C., Moraes, O. L. L., Degrazia, G. A., and Medeiros, L. E.: Intermittency and the Exchange of Scalars in the Nocturnal Surface Layer, Boundary-Layer Meteorology, 119, 41–55, https://doi.org/10.1007/s10546-005-9019-3, 2006.

Acevedo, O. C., Mahrt, L., Puhales, F. S., Costa, F. D., Medeiros, L. E., and Degrazia, G. A.: Contrasting structures between the decoupled and coupled states of the stable boundary layer: Stable Boundary Layer Coupling, Quarterly Journal of the Royal Meteorological Society, 142, 693–702, https://doi.org/10.1002/qj.2693, 2016.

Acevedo, O. C., Maroneze, R., Costa, F. D., Puhales, F. S., Degrazia, G. A., Martins, L. G. N., Oliveira, P. E. S., and Mortarini, L.: The Nocturnal Boundary Layer transition from Weakly to Very Stable. Part 1. Observations, Quaterly Journal of the Royal Meteorological Society, https://doi.org/10.1002/qj.3642, 2019.

Akagi, S. K., Yokelson, R. J., Wiedinmyer, C., Alvarado, M. J., Reid, J. S., Karl, T., Crounse, J. D., and Wennberg, P. O.: Emission factors for open and domestic biomass burning for use in atmospheric models, Atmospheric Chemistry and Physics, 11, 4039–4072, https://doi.org/10.5194/acp-11-4039-2011, 2011.

Andreae, M. O.: Emission of trace gases and aerosols from biomass burning – an updated assessment, Atmospheric Chemistry and Physics, 19, 8523–8546, https://doi.org/10.5194/acp-19-8523-2019, 2019.

Andreae, M. O. and Merlet, P.: Emission of trace gases and aerosols from biomass burning, Global Biogeochemical Cycles, 15, 955–966, https://doi.org/10.1029/2000GB001382, 2001.

Andreae, M. O., Artaxo, P., Beck, V., Bela, M., Freitas, S., Gerbig, C., Longo, K., Munger, J. W., Wiedemann, K. T., and Wofsy, S. C.: Carbon monoxide and related trace gases and aerosols over the Amazon Basin during the wet and dry seasons, Atmospheric Chemistry and Physics, 12, 6041–6065, https://doi.org/10.5194/acp-12-6041-2012, 2012.

Andreae, M. O., Acevedo, O. C., Araùjo, A., Artaxo, P., Barbosa, C. G. G., Barbosa, H. M. J., Brito, J., Carbone, S., Chi, X., Cintra, B. B. L., da Silva, N. F., Dias, N. L., Dias-Júnior, C. Q., Ditas, F., Ditz, R., Godoi, A. F. L., Godoi, R. H. M., Heimann, M., Hoffmann, T., Kesselmeier, J., Könemann, T., Krüger, M. L., Lavric, J. V., Manzi, A. O., Lopes, A. P., Martins, D. L., Mikhailov, E. F., Moran-Zuloaga, D., Nelson, B. W., Nölscher, A. C., Santos Nogueira, D., Piedade, M. T. F., Pöhlker, C., Pöschl, U., Quesada, C. A., Rizzo, L. V., Ro, C.-U., Ruckteschler, N., Sá, L. D. A., de Oliveira Sá, M., Sales, C. B., dos Santos, R. M. N., Saturno, J., Schöngart, J., Sörgel, M., de Souza, C. M., de Souza, R. A. F., Su, H., Targhetta, N., Tóta, J., Trebs, I., Trumbore, S., van Eijck, A., Walter, D., Wang, Z., Weber, B., Williams, J., Winderlich, J., Wittmann, F., Wolff, S., and Yáñez-Serrano, A. M.: The Amazon Tall Tower Observatory (ATTO): overview of pilot measurements on ecosystem ecology, meteorology, trace gases, and aerosols, Atmospheric Chemistry and Physics, 15, 10 723–10 776, https://doi.org/10.5194/acp-15-10723-2015, 2015.

Aragão, L. E. O. C., Anderson, L. O., Fonseca, M. G., Rosan, T. M., Vedovato, L. B., Wagner, F. H., Silva, C. V. J., Junior, C. H. L. S., Arai, E., Aguiar, A. P., Barlow, J., Berenguer, E., Deeter, M. N., Domingues, L. G., Gatti, L., Gloor, M., Malhi, Y., Marengo, J. A., Miller, J. B., Phillips, O. L., and Saatchi, S.: 21st Century drought-related fires counteract the decline of Amazon deforestation carbon emissions, Nature Communications, 9, 1–12, https://doi.org/10.1038/s41467-017-02771-y, 2018.

Araújo, A. C. d., Kruijt, B., Nobre, A. D., Dolman, A. J., Waterloo, M. J., Moors, E. J., and Souza, J. S. d.: Nocturnal accumulation of CO2 underneath a tropical forest canopy along a topographical gradient, Ecological Applications, 18, 1406–1419, https://doi.org/10.1890/06-0982.1, 2008.

Assahira, C., Piedade, M. T. F., Trumbore, S. E., Wittmann, F., Cintra, B. B. L., Batista, E. S., Resende, A. F. d., and Schöngart, J.: Tree mortality of a flood-adapted species in response of hydrographic changes caused by an Amazonian river dam, Forest Ecology and Management, 396, 113–123, https://doi.org/10.1016/j.foreco.2017.04.016, 2017.

Beck, V., Chen, H., Gerbig, C., Bergamaschi, P., Bruhwiler, L., Houweling, S., Röckmann, T., Kolle, O., Steinbach, J., Koch, T., Sapart, C. J., van der Veen, C., Frankenberg, C., Andreae, M. O., Artaxo, P., Longo, K. M., and Wofsy, S. C.: Methane airborne measurements and comparison to global models during BARCA, Journal of Geophysical Research: Atmospheres, 117, https://doi.org/10.1029/2011JD017345, 2012.

Bloom, A. A., Palmer, P. I., Fraser, A., and Reay, D. S.: Seasonal variability of tropical wetland CH4 emissions: the role of the methanogen-available carbon pool, Biogeosciences, 9, 2821–2830, https://doi.org/10.5194/bg-9-2821-2012, 2012.

Bloom, A. A., Bowman, K. W., Lee, M., Turner, A. J., Schroeder, R., Worden, J. R., Weidner, R., McDonald, K. C., and Jacob, D. J.: A global wetland methane emissions and uncertainty dataset for atmospheric chemical transport models (WetCHARTs version 1.0), Geoscientific Model Development, 10, 2141–2156, https://doi.org/10.5194/gmd-10-2141-2017, 2017.

Carmo, J. B. d., Keller, M., Dias, J. D., Camargo, P. B. d., and Crill, P.: A source of methane from upland forests in the Brazilian Amazon, Geophysical Research Letters, 33, https://doi.org/10.1029/2005GL025436, https://agupubs.onlinelibrary.wiley.com/doi/abs/10.1029/2005GL025436, 2006.

Carneiro, R. G.: Erosão da Camada Limite Noturna e suas Implicações no Crescimento da Camada Limite Convectiva na Região Central da Amazônia (Experimento GoAmazon 2014/5), Ph.D. thesis, Instituto Nacional de Pesquisas Espaciais (INPE), 2018.

Carslaw, D. C. and Ropkins, K.: openair — An R package for air quality data analysis, Environmental Modelling & Software, 27-28, 52–61, https://doi.org/10.1016/j.envsoft.2011.09.008, 2012.

Carslaw, K. S., Boucher, O., Spracklen, D. V., Mann, G. W., Rae, J. G. L., Woodward, S., and Kulmala, M.: A review of natural aerosol interactions and feedbacks within the Earth system, Atmospheric Chemistry and Physics, 10, 1701–1737, https://doi.org/10.5194/acp-10-1701-2010, 2010.

Cava, D., Giostra, U., Siqueira, M., and Katul, G.: Organised Motion and Radiative Perturbations in the Nocturnal Canopy Sublayer above an Even-Aged Pine Forest, Boundary-Layer Meteorology, 112, 129–157, https://doi.org/10.1023/B:BOUN.0000020160.28184.a0, 2004.

Ciais, P., Sabine, C., Bala, G., Bopp, L., Brovkin, V., Canadell, J. G., Chhabra, A., DeFries, R., Galloway, J., Heimann, M., Jones, C., Le Queré, C., Myneni, R., Piao, S., and Thornton, P.: Carbon and Other Biogeochemical Cycles. In: Climate Change 2013: The Physical Science Basis. Contribution of Working Group I to the Fifth Assessment Report of the Intergovernmental Panel on Climate Change [Stocker, T.F., D. Qin, G.-K. Plattner, M. Tignor, S.K. Allen, J. Boschung, A. Nauels, Y. Xia, V. Bex and P.M. Midgley (eds.)]., in: IPCC AR5 Report, Cambridge University Press, Cambridge, United Kingdom and New York, NY, USA., 2013.

De Oliveira, A. P. and Fitzjarrald, D. R.: The Amazon river breeze and the local boundary layer: II. Linear analysis and modelling, Boundary-Layer Meteorology, 67, 75–96, https://doi.org/10.1007/BF00705508, 1994.

Dias-Junior, C. Q., Sá, L. D., Marques Filho, E. P., Santana, R. A., Mauder, M., and Manzi, A. O.: Turbulence regimes in the stable boundary layer above and within the Amazon forest, Agricultural and Forest Meteorology, 233, 122–132, https://doi.org/10.1016/j.agrformet.2016.11.001, 2017.

Dias-Júnior, C. Q., Dias, N. L., Santos, R. M. N. d., Sörgel, M., Araújo, A., Tsokankunku, A., Ditas, F., Santana, R. A. d., Randow, C. v., Sá, M., Pöhlker, C., Machado, L. A. T., Sá, L. D. d., Moran-Zuloaga, D., Janssen, R., Acevedo, O., Oliveira, P., Fisch, G., Chor, T., and Manzi, A.: Is There a Classical Inertial Sublayer Over the Amazon Forest?, Geophysical Research Letters, 46, 5614–5622, https://doi.org/10.1029/2019GL083237, 2019.

Dlugokencky, E. and NOAA: www.esrl.noaa.gov/gmd/ccgg/trends_ch4/.

Dlugokencky E., Nisbet Euan G., Fisher Rebecca, and Lowry David: Global atmospheric methane: budget, changes and dangers, Philosophical Transactions of the Royal Society A: Mathematical, Physical and Engineering Sciences, 369, 2058–2072, https://doi.org/10.1098/rsta.2010.0341, 2011.

5 Dutaur, L. and Verchot, L. V.: A global inventory of the soil CH4 sink, Global Biogeochemical Cycles, 21, https://doi.org/10.1029/2006GB002734, https://agupubs.onlinelibrary.wiley.com/doi/abs/10.1029/2006GB002734, 2007.

Dörr, H., Katruff, L., and Levin, I.: Soil texture parameterization of the methane uptake in aerated soils, Chemosphere, 26, 697–713, https://doi.org/10.1016/0045-6535(93)90454-D, 1993.

Fisch, G., Tota, J., Machado, L. A. T., Silva Dias, M. A. F., da F. Lyra, R. F., Nobre, C. A., Dolman, A. J., and Gash, J. H. C.: The convective
10 boundary layer over pasture and forest in Amazonia, Theoretical and Applied Climatology, 78, https://doi.org/10.1007/s00704-004-0043-x, 2004.

Fitzjarrald, D. R. and Moore, K. E.: Mechanisms of nocturnal exchange between the rain forest and the atmosphere, Journal of Geophysical Research, 95, 16 839, https://doi.org/10.1029/JD095iD10p16839, 1990.

Gatti, L. V., Gloor, M., Miller, J. B., Doughty, C. E., Malhi, Y., Domingues, L. G., Basso, L. S., Martinewski, A., Correia, C. S. C., Borges,
15 V. F., Freitas, S., Braz, R., Anderson, L. O., Rocha, H., Grace, J., Phillips, O. L., and Lloyd, J.: Drought sensitivity of Amazonian carbon balance revealed by atmospheric measurements, Nature, 506, 76–80, https://doi.org/10.1038/nature12957, 2014.

Gloor, M., Bakwin, P., Hurst, D., Lock, L., Draxler, R., and Tans, P.: What is the concentration footprint of a tall tower?, Journal of Geophysical Research: Atmospheres, 106, 17 831–17 840, https://doi.org/10.1029/2001JD900021, 2001.

Goulden, M. L., Miller, S. D., and Rocha, H. R. d.: Nocturnal cold air drainage and pooling in a tropical forest, Journal of Geophysical
20 Research: Atmospheres, 111, https://doi.org/10.1029/2005JD006037, 2006.

Howarth, R. W.: Ideas and perspectives: is shale gas a major driver of recent increase in global atmospheric methane?, Biogeosciences, 16, 3033–3046, https://doi.org/https://doi.org/10.5194/bg-16-3033-2019, 2019.

Högström, U.: Analysis of Turbulence Structure in the Surface Layer with a Modified Similarity Formulation for Near Neutral Conditions, Journal of the atmospheric sciences, 47, 1949–1972, 1990.

25 Junk, W. J., Piedade, M. T. F., Schöngart, J., Cohn-Haft, M., Adeney, J. M., and Wittmann, F.: A Classification of Major Naturally-Occurring Amazonian Lowland Wetlands, Wetlands, 31, 623–640, https://doi.org/10.1007/s13157-011-0190-7, 2011.

Kaplan, J. O.: Wetlands at the Last Glacial Maximum: Distribution and methane emissions, Geophysical Research Letters, 29, 3–1–3–4, https://doi.org/10.1029/2001GL013366, 2002.

Karipot, A., Leclerc, M. Y., Zhang, G., Lewin, K. F., Nagy, J., Hendrey, G. R., and Starr, G.: Influence of nocturnal low-level jet
30 on turbulence structure and CO2 flux measurements over a forest canopy, Journal of Geophysical Research: Atmospheres, 113, https://doi.org/10.1029/2007JD009149, 2008.

Kemenes, A., Forsberg, B. R., and Melack, J. M.: Methane release below a tropical hydroelectric dam, Geophysical Research Letters, 34, https://doi.org/10.1029/2007GL029479, 2007.

Kirschke, S., Bousquet, P., Ciais, P., Saunois, M., Canadell, J. G., Dlugokencky, E. J., Bergamaschi, P., Bergmann, D., Blake, D. R., Bruhwiler,
35 L., Cameron-Smith, P., Castaldi, S., Chevallier, F., Feng, L., Fraser, A., Heimann, M., Hodson, E. L., Houweling, S., Josse, B., Fraser, P. J., Krummel, P. B., Lamarque, J.-F., Langenfelds, R. L., Le Quéré, C., Naik, V., O'Doherty, S., Palmer, P. I., Pison, I., Plummer, D., Poulter, B., Prinn, R. G., Rigby, M., Ringeval, B., Santini, M., Schmidt, M., Shindell, D. T., Simpson, I. J., Spahni, R., Steele, L. P., Strode, S. A.,

Sudo, K., Szopa, S., van der Werf, G. R., Voulgarakis, A., van Weele, M., Weiss, R. F., Williams, J. E., and Zeng, G.: Three decades of global methane sources and sinks, Nature Geoscience, 6, 813–823, https://doi.org/10.1038/ngeo1955, 2013.

Klein, V. P. and Piedade, M. T. F.: Orchidaceae occurring in white-sand ecosystems of the Uatumã Sustainable Development Reserve in Central Amazon, Phytotaxa, 419, 113–148, https://doi.org/10.11646/phytotaxa.419.2.1, 2019.

5 Kruijt, B., Malhi, Y., Lloyd, J., Norbre, A. D., Miranda, A. C., Pereira, M. G. P., Culf, A., and Grace, J.: Turbulence Statistics Above And Within Two Amazon Rain Forest Canopies, Boundary-Layer Meteorology, 94, 297–331, https://doi.org/10.1023/A:1002401829007, 2000.

Mahrt, L.: Characteristics of Submeso Winds in the Stable Boundary Layer, Boundary-Layer Meteorology, 130, 1–14, https://doi.org/10.1007/s10546-008-9336-4, 2009.

Marht, L., Thomas, C., Richardson, S., Seaman, N., Stauffer, D., and Zeeman, M.: Non-stationary Generation of Weak Turbulence for Very
10 Stable and Weak-Wind Conditions, Boundary Layer Meteorology, pp. 179–199, https://doi.org/10.1007/s10546-012-9782-x, 2013.

Martin, S. T., Artaxo, P., Machado, L. A. T., Manzi, A. O., Souza, R. A. F., Schumacher, C., Wang, J., Andreae, M. O., Barbosa, H. M. J., Fan, J., Fisch, G., Goldstein, A. H., Guenther, A., Jimenez, J. L., Pöschl, U., Silva Dias, M. A., Smith, J. N., and Wendisch, M.: Introduction: Observations and Modeling of the Green Ocean Amazon (GoAmazon2014/5), Atmospheric Chemistry and Physics, 16, 4785–4797, https://doi.org/10.5194/acp-16-4785-2016, 2016.

15 Melton, J. R., Wania, R., Hodson, E. L., Poulter, B., Ringeval, B., Spahni, R., Bohn, T., Avis, C. A., Beerling, D. J., Chen, G., Eliseev, A. V., Denisov, S. N., Hopcroft, P. O., Lettenmaier, D. P., Riley, W. J., Singarayer, J. S., Subin, Z. M., Tian, H., Zürcher, S., Brovkin, V., van Bodegom, P. M., Kleinen, T., Yu, Z. C., and Kaplan, J. O.: Present state of global wetland extent and wetland methane modelling: conclusions from a model inter-comparison project (WETCHIMP), Biogeosciences, 10, 753–788, https://doi.org/10.5194/bg-10-753-2013, 2013.

20 Miller, J. B., Gatti, L. V., d'Amelio, M. T. S., Crotwell, A. M., Dlugokencky, E. J., Bakwin, P., Artaxo, P., and Tans, P. P.: Airborne measurements indicate large methane emissions from the eastern Amazon basin, Geophysical Research Letters, 34, https://doi.org/10.1029/2006GL029213, 2007.

NASA-JPL: NASA Shuttle Radar Topography Mission Global 1 arc second [Data set]. NASA EOSDIS Land Processes DAAC, 2013.

Nisbet, E. G., Dlugokencky, E. J., Manning, M. R., Lowry, D., Fisher, R. E., France, J. L., Michel, S. E., Miller, J. B., White, J. W. C., Vaughn,
25 B., Bousquet, P., Pyle, J. A., Warwick, N. J., Cain, M., Brownlow, R., Zazzeri, G., Lanoisellé, M., Manning, A. C., Gloor, E., Worthy, D. E. J., Brunke, E.-G., Labuschagne, C., Wolff, E. W., and Ganesan, A. L.: Rising atmospheric methane: 2007-2014 growth and isotopic shift, Global Biogeochemical Cycles, 30, 1356–1370, https://doi.org/10.1002/2016GB005406, http://doi.wiley.com/10.1002/2016GB005406, 2016.

Oliveira, P. E. S., Acevedo, O. C., Sörgel, M., Tsokankunku, A., Wolff, S., Araújo, A. C., Souza, R. A. F., Sá, M. O., Manzi, A. O., and
30 Andreae, M. O.: Nighttime wind and scalar variability within and above an Amazonian canopy, Atmospheric Chemistry and Physics, 18, 3083–3099, https://doi.org/10.5194/acp-18-3083-2018, 2018.

Pangala, S. R., Enrich-Prast, A., Basso, L. S., Peixoto, R. B., Bastviken, D., Hornibrook, E. R. C., Gatti, L. V., Ribeiro, H., Calazans, L. S. B., Sakuragui, C. M., Bastos, W. R., Malm, O., Gloor, E., Miller, J. B., and Gauci, V.: Large emissions from floodplain trees close the Amazon methane budget, Nature, https://doi.org/10.1038/nature24639, 2017.

35 Pfannerstill, E. Y., Nölscher, A. C., Yáñez-Serrano, A. M., Bourtsoukidis, E., Keßel, S., Janssen, R. H. H., Tsokankunku, A., Wolff, S., Sörgel, M., Sá, M. O., Araújo, A., Walter, D., Lavrič, J., Dias-Júnior, C. Q., Kesselmeier, J., and Williams, J.: Total OH Reactivity Changes Over the Amazon Rainforest During an El Niño Event, Frontiers in Forests and Global Change, 1, https://doi.org/10.3389/ffgc.2018.00012, 2018.

Pöhlker, C., Walter, D., Paulsen, H., Könemann, T., Rodríguez-Caballero, E., Moran-Zuloaga, D., Brito, J., Carbone, S., Degrendele, C., Després, V. R., Ditas, F., Holanda, B. A., Kaiser, J. W., Lammel, G., Lavrič, J. V., Ming, J., Pickersgill, D., Pöhlker, M. L., Praß, M., Löbs, N., Saturno, J., Sörgel, M., Wang, Q., Weber, B., Wolff, S., Artaxo, P., Pöschl, U., and Andreae, M. O.: Land cover and its transformation in the backward trajectory footprint region of the Amazon Tall Tower Observatory, Atmospheric Chemistry and Physics, 19, 8425–8470, https://doi.org/10.5194/acp-19-8425-2019, 2019.

Querino, C. A. S., Smeets, C. J. P. P., Vigano, I., Holzinger, R., Moura, V., Gatti, L. V., Martinewski, A., Manzi, A. O., de Araújo, A. C., and Röckmann, T.: Methane flux, vertical gradient and mixing ratio measurements in a tropical forest, Atmospheric Chemistry and Physics, 11, 7943–7953, https://doi.org/10.5194/acp-11-7943-2011, 2011.

Resende, A. F. d., Schöngart, J., Streher, A. S., Ferreira-Ferreira, J., Piedade, M. T. F., and Silva, T. S. F.: Massive tree mortality from flood pulse disturbances in Amazonian floodplain forests: The collateral effects of hydropower production, Science of The Total Environment, 659, 587–598, https://doi.org/10.1016/j.scitotenv.2018.12.208, 2019.

Richey, J. E., Devol, A. H., Wofsy, S. C., Victoria, R., and Riberio, M. N. G.: Biogenic gases and the oxidation and reduction of carbon in Amazon River and floodplain waters: Amazon dissolved gases, Limnology and Oceanography, 33, 551–561, https://doi.org/10.4319/lo.1988.33.4.0551, 1988.

Rigby, M., Montzka, S. A., Prinn, R. G., White, J. W. C., Young, D., O'Doherty, S., Lunt, M. F., Ganesan, A. L., Manning, A. J., Simmonds, P. G., Salameh, P. K., Harth, C. M., Mühle, J., Weiss, R. F., Fraser, P. J., Steele, L. P., Krummel, P. B., McCulloch, A., and Park, S.: Role of atmospheric oxidation in recent methane growth, Proceedings of the National Academy of Sciences, 114, 5373–5377, https://doi.org/10.1073/pnas.1616426114, 2017.

Ringeval, B., Houweling, S., van Bodegom, P. M., Spahni, R., van Beek, R., Joos, F., and Röckmann, T.: Methane emissions from floodplains in the Amazon Basin: challenges in developing a process-based model for global applications, Biogeosciences, 11, 1519–1558, https://doi.org/10.5194/bg-11-1519-2014, 2014.

Sanderson, M. G.: Biomass of termites and their emissions of methane and carbon dioxide: A global database, Global Biogeochemical Cycles, 10, 543–557, https://doi.org/10.1029/96GB01893, 1996.

Saturno, J., Holanda, B. A., Pöhlker, C., Ditas, F., Wang, Q., Moran-Zuloaga, D., Brito, J., Carbone, S., Cheng, Y., Chi, X., Ditas, J., Hoffmann, T., Hrabe de Angelis, I., Könemann, T., Lavrič, J. V., Ma, N., Ming, J., Paulsen, H., Pöhlker, M. L., Rizzo, L. V., Schlag, P., Su, H., Walter, D., Wolff, S., Zhang, Y., Artaxo, P., Pöschl, U., and Andreae, M. O.: Black and brown carbon over central Amazonia: long-term aerosol measurements at the ATTO site, Atmospheric Chemistry and Physics, 18, 12 817–12 843, https://doi.org/10.5194/acp-18-12817-2018, 2018.

Saunois, M., Bousquet, P., Poulter, B., Peregon, A., Ciais, P., Canadell, J. G., Dlugokencky, E. J., Etiope, G., Bastviken, D., Houweling, S., Janssens-Maenhout, G., Tubiello, F. N., Castaldi, S., Jackson, R. B., Alexe, M., Arora, V. K., Beerling, D. J., Bergamaschi, P., Blake, D. R., Brailsford, G., Brovkin, V., Bruhwiler, L., Crevoisier, C., Crill, P., Covey, K., Curry, C., Frankenberg, C., Gedney, N., Höglund-Isaksson, L., Ishizawa, M., Ito, A., Joos, F., Kim, H.-S., Kleinen, T., Krummel, P., Lamarque, J.-F., Langenfelds, R., Locatelli, R., Machida, T., Maksyutov, S., McDonald, K. C., Marshall, J., Melton, J. R., Morino, I., Naik, V., O'Doherty, S., Parmentier, F.-J. W., Patra, P. K., Peng, C., Peng, S., Peters, G. P., Pison, I., Prigent, C., Prinn, R., Ramonet, M., Riley, W. J., Saito, M., Santini, M., Schroeder, R., Simpson, I. J., Spahni, R., Steele, P., Takizawa, A., Thornton, B. F., Tian, H., Tohjima, Y., Viovy, N., Voulgarakis, A., van Weele, M., van der Werf, G. R., Weiss, R., Wiedinmyer, C., Wilton, D. J., Wiltshire, A., Worthy, D., Wunch, D., Xu, X., Yoshida, Y., Zhang, B., Zhang, Z., and Zhu, Q.: The global methane budget 2000–2012, Earth System Science Data, 8, 697–751, https://doi.org/10.5194/essd-8-697-2016, 2016.

Sawakuchi, H. O., Bastviken, D., Sawakuchi, A. O., Krusche, A. V., Ballester, M. V. R., and Richey, J. E.: Methane emissions from Amazonian Rivers and their contribution to the global methane budget, Global Change Biology, 20, 2829–2840, https://doi.org/10.1111/gcb.12646, 2014.

Schaefer, H., Fletcher, S. E. M., Veidt, C., Lassey, K. R., Brailsford, G. W., Bromley, T. M., Dlugokencky, E. J., Michel, S. E., Miller, J. B., Levin, I., Lowe, D. C., Martin, R. J., Vaughn, B. H., and White, J. W. C.: A 21st-century shift from fossil-fuel to biogenic methane emissions indicated by 13CH4, Science, 352, 80–84, https://doi.org/10.1126/science.aad2705, 2016.

Schjønning, P., McBride, R., Keller, T., and Obour, P.: Predicting soil particle density from clay and soil organic matter contents, Geoderma, 286, 83–87, https://doi.org/10.1016/j.geoderma.2016.10.020, 2017.

Stull, R. B.: An introduction to Boundary Layer Mateorology, Kluwer Academic Publishers, 1988.

Sun, J., Desjardins, R., Mahrt, L., and MacPherson, I.: Transport of carbon dioxide, water vapor, and ozone by turbulence and local circulations, Journal of Geophysical Research: Atmospheres, 103, 25 873–25 885, https://doi.org/10.1029/98JD02439, 1998.

Sun, J., Mahrt, L., Banta, R. M., and Pichugina, Y. L.: Turbulence Regimes and Turbulence Intermittency in the Stable Boundary Layer during CASES-99, Journal of the Atmospheric Sciences, 69, 338–351, https://doi.org/10.1175/JAS-D-11-082.1, 2012.

Turner, A. J., Frankenberg, C., Wennberg, P. O., and Jacob, D. J.: Ambiguity in the causes for decadal trends in atmospheric methane and hydroxyl, Proceedings of the National Academy of Sciences, 114, 5367–5372, https://doi.org/10.1073/pnas.1616020114, 2017.

Turner, A. J., Frankenberg, C., and Kort, E. A.: Interpreting contemporary trends in atmospheric methane, Proceedings of the National Academy of Sciences, 116, 2805–2813, https://doi.org/10.1073/pnas.1814297116, 2019.

Tóta, J., Fitzjarrald, D. R., Staebler, R. M., Sakai, R. K., Moraes, O. M. M., Acevedo, O. C., Wofsy, S. C., and Manzi, A. O.: Amazon rain forest subcanopy flow and the carbon budget: Santarém LBA-ECO site, Journal of Geophysical Research: Biogeosciences, 113, https://doi.org/10.1029/2007JG000597, 2008.

Tóta, J., Roy Fitzjarrald, D., and da Silva Dias, M. A. F.: Amazon Rainforest Exchange of Carbon and Subcanopy Air Flow: Manaus LBA Site—A Complex Terrain Condition, The Scientific World Journal, 2012, 1–19, https://doi.org/10.1100/2012/165067, 2012.

Vale, R., Santana, R., Gomes, A. C., and Tóta, J.: Increased nocturnal CO2 concentration during breeze circulation events in a tropical reservoir, Ambiente e Agua - An Interdisciplinary Journal of Applied Science, 13, 1, https://doi.org/10.4136/ambi-agua.2186, 2018.

van der Laan-Luijkx, I. T., van der Velde, I. R., Krol, M. C., Gatti, L. V., Domingues, L. G., Correia, C. S. C., Miller, J. B., Gloor, M., van Leeuwen, T. T., Kaiser, J. W., Wiedinmyer, C., Basu, S., Clerbaux, C., and Peters, W.: Response of the Amazon carbon balance to the 2010 drought derived with CarbonTracker South America, Global Biogeochemical Cycles, 29, 1092–1108, https://doi.org/10.1002/2014GB005082, 2015.

Verchot, L. V., Davidson, E. A., Cattânio, J. H., and Ackerman, I. L.: Land-Use Change and Biogeochemical Controls of Methane Fluxes in Soils of Eastern Amazonia, Ecosystems, 3, 41–56, https://doi.org/10.1007/s100210000009, 2000.

Webb, A. J., Bösch, H., Parker, R. J., Gatti, L. V., Gloor, E., Palmer, P. I., Basso, L. S., Chipperfield, M. P., Correia, C. S. C., Domingues, L. G., Feng, L., Gonzi, S., Miller, J. B., Warneke, T., and Wilson, C.: CH4 concentrations over the Amazon from GOSAT consistent with in situ vertical profile data, Journal of Geophysical Research: Atmospheres, 121, 11,006–11,020, https://doi.org/10.1002/2016JD025263, 2016.

Welch, B., Gauci, V., and Sayer, E. J.: Tree stem bases are sources of CH_4 and N_2O in a tropical forest on upland soil during the dry to wet season transition, Global Change Biology, 25, 361–372, https://doi.org/10.1111/gcb.14498, 2019.

Wiegner, M. and Geiß, A.: Aerosol profiling with the Jenoptik ceilometer CHM15kx, Atmospheric Measurement Techniques, 5, 1953–1964, https://doi.org/10.5194/amt-5-1953-2012, 2012.

Wilson, C., Gloor, M., Gatti, L. V., Miller, J. B., Monks, S. A., McNorton, J., Bloom, A. A., Basso, L. S., and Chipperfield, M. P.: Contribution of regional sources to atmospheric methane over the Amazon Basin in 2010 and 2011., Global Biogeochemical Cycles, 30, 400–420, https://doi.org/10.1002/2015GB005300, 2016.

Winderlich, J., Chen, H., Gerbig, C., Seifert, T., Kolle, O., Lavrič, J. V., Kaiser, C., Höfer, A., and Heimann, M.: Continuous low-maintenance CO_2/CH_4/H_2O measurements at the Zotino Tall Tower Observatory (ZOTTO) in Central Siberia, Atmospheric Measurement Techniques, 3, 1113–1128, https://doi.org/10.5194/amt-3-1113-2010, 2010.

Zeri, M. and Sá, L. D. A.: Horizontal and Vertical Turbulent Fluxes Forced by a Gravity Wave Event in the Nocturnal Atmospheric Surface Layer Over the Amazon Forest, Boundary-Layer Meteorology, 138, 413–431, https://doi.org/10.1007/s10546-010-9563-3, 2011.

5

Table 1. Observational data used in each of the sections. We specify the time resolution and the period of time used. ~~Met. data stands for meteorological data and refers to the variables described in Sect 2.3~~

Sections	Data used	Time resolution	Period of time
3.2, 3.3.1, 3.3.2	CH_4 mixing ratios	30 min	2013-06 to 2018-11
	~~Met.~~ Meteorological data	30 min	2013-06 to 2018-11
3.3.3	CH_4 mixing ratios	15 min	2014: March, April, May, July, August, September
	~~Met.~~ Meteorological data	10 Hz (avg. to 1 min)	2014: March, April, May, July, August, September
3.4	CH_4 mixing ratios	30 min	2013-06 to 2018-11
	CO mixing ratios in CH4:CO	30 min	2013-06 to 2018-11
	CO mixing ratios in BC:CO	30 min	~~2014-01 to 2015-12~~ 2013-06 to 2018-05
	Black Carbon	30 min	~~2014-01 to 2015-12~~ 2013-06 to 2018-05

~~Percentage of nighttime positive gradient occurrences for different 1/L classes. The 1/L classes were defined based on Kruijt et al. (2000). Note that the percentages do not add to 100% because the upper and lower boundaries of the classes are based on Q1, Q3 ± 1.5 * inter-quartile range (IQR).~~

5 ~~Positive Gradients Events (%) Q1 - 1.5 * IQR < 1/L < -0.1 - Very unstable 9.3 -0.1 < 1/L < -0.01 - Moderately unstable 12.1 -0.01 < 1/L < 0.01 - Neutral 6.7 0.01 < 1/L < 0.1 - Moderately stable 26.7 0.1 < 1/L < Q3 + 1.5 * IQR - Very stable 22.4~~
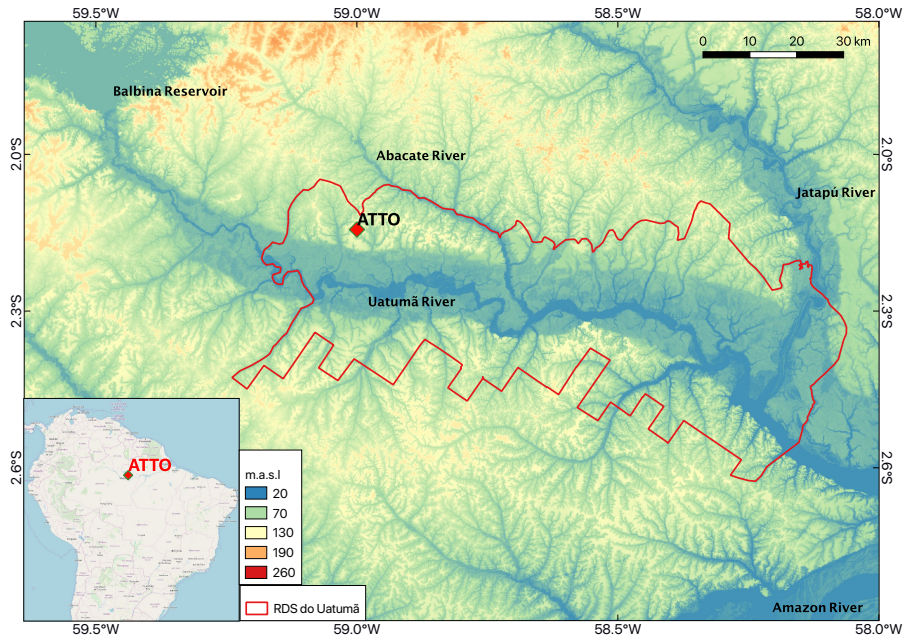
Figure 1. Location of ATTO relative to the continent. The topography, in the background, is based on the elevation model from the Shuttle Radar Topography Mission (NASA-JPL, 2013). The boundaries of the Uatumã Sustainable Development Reserve (USDR) are highlighted in the red polygon and the major rivers are labelled.
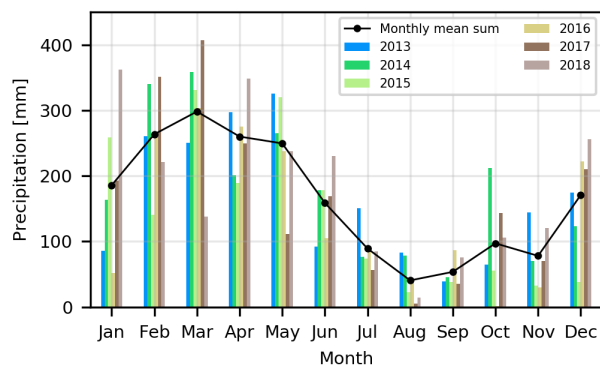
Figure 2. Monthly sums of precipitation for the period between 2013-2018 at ATTO.
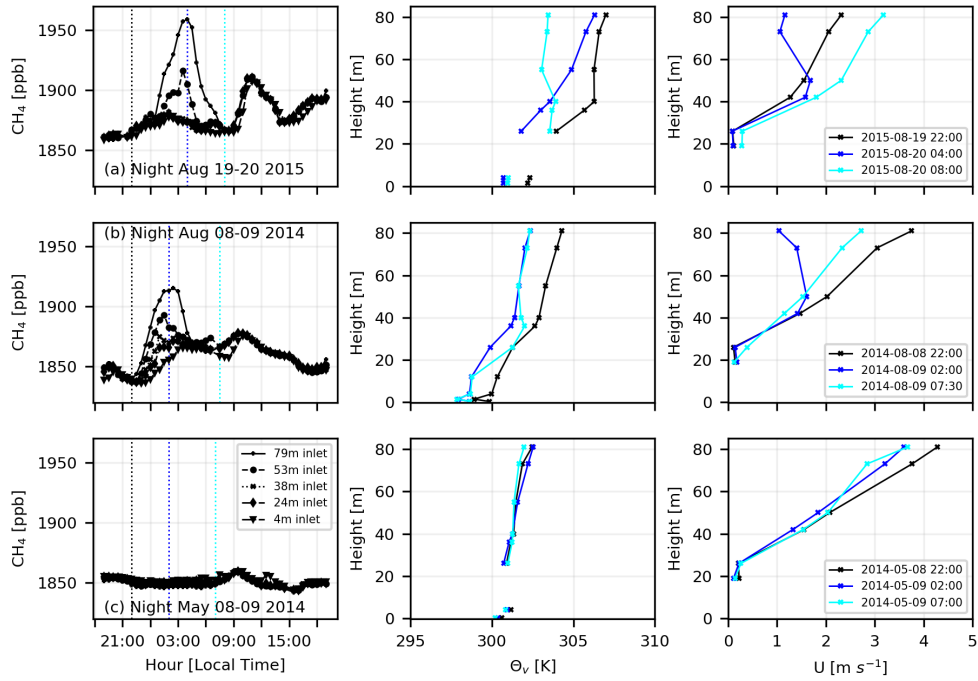
Figure 3. CH$_4$ time series for three selected nights (first column) showing a 24-hour interval, virtual potential temperature (second column) and mean wind profiles (third column) for three selected periods of the CH$_4$ time series. The times at which the profiles are plotted are highlighted on the CH$_4$ time series with the same colors. The canopy height is approximately 35 m. Note that due to instrument malfunctioning the Θ_v profiles are lacking data at 12 m. The wind speed profiles cover from 19 m to 81 m.
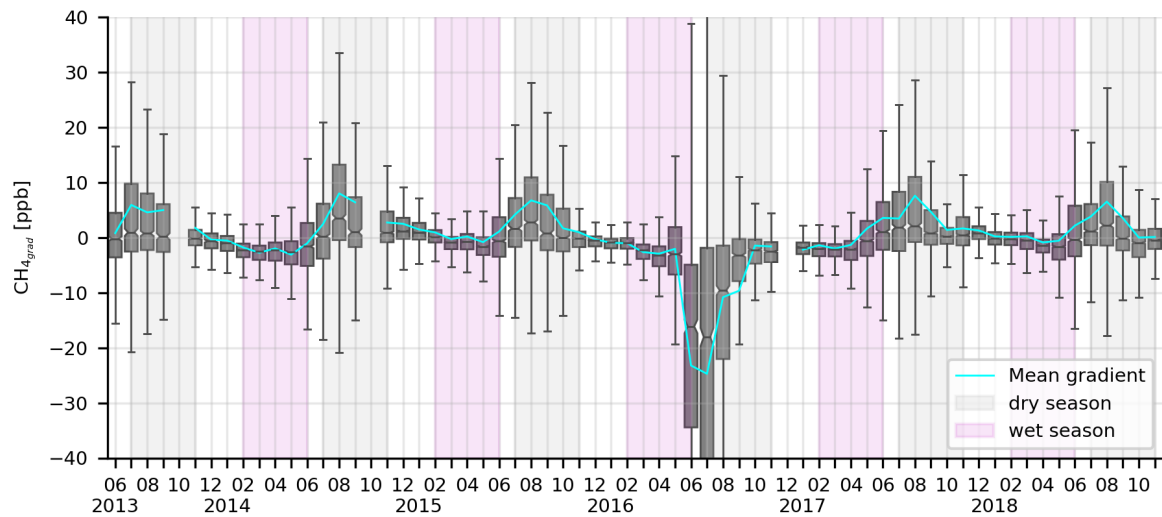
Figure 4. Monthly box-and-whisker plot of CH_4 gradient between the 79 m and 4 m levels. The box denotes the inter-quartile range (IQR), showing the median with a notched line. The whiskers range from Q1-1.5*IQR to Q3+1.5*IQR, with Q1 and Q3 being the 25th and 75th percentiles. The cyan line is the monthly mean gradient. The monthly statistics are calculated from half-hourly measurements at ATTO.
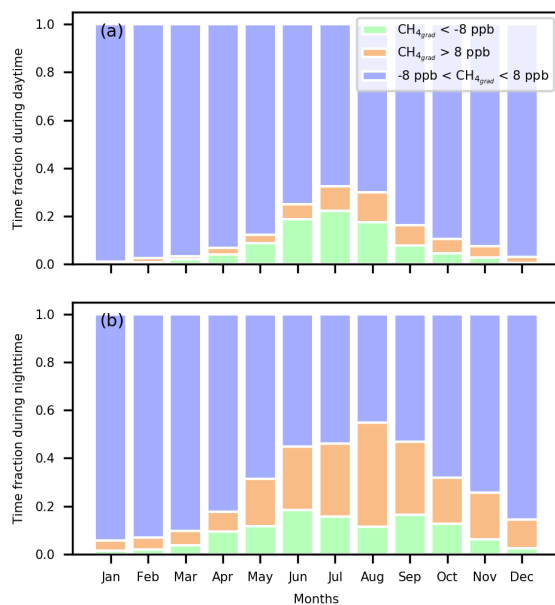
Figure 5. Time fractions for daytime (a) and nighttime (b) measurements in which $CH_{4grad} > 8$ ppb, $-8 < CH_{4grad} < 8$ ppb and $CH_{4grad} < -8$ ppb. Nighttime is defined as between 20:00 and 06:00 and daytime as between ~~06~~07:00 and 18:00, local time.
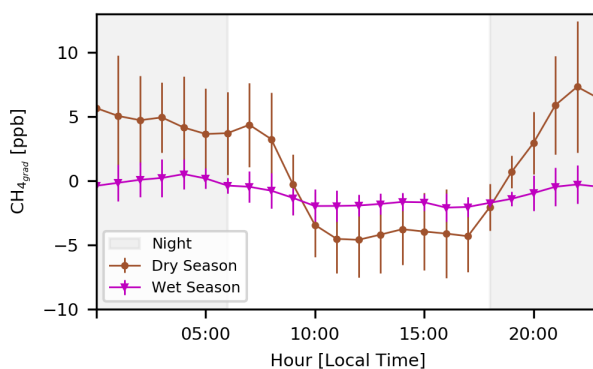
Figure 6. Mean diurnal cycle of the CH_4 gradient between the 79 m and 4 m levels. The period between June 2013 and November 2018 was used and separated by dry and wet seasons. The error bars show the standard deviations~~.~~

Figure 7. Mean CH₄ gradient for each bin of wind direction and time of day (left panel) or month of the year (right panel). Wind direction measured at 81 m and CH₄ mixing ratios at 79 m. Plot produced in R with the Openair package (Carslaw and Ropkins, 2012) (Carslaw et al., 2010)
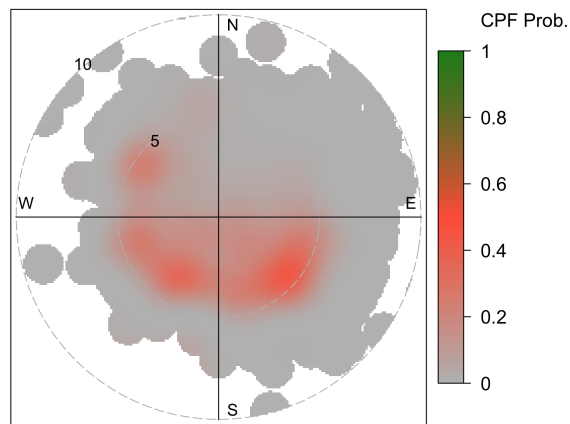
Figure 8. Polar plot showing the conditional probability function (CPF) of the gradients above 8 ppb (88th to 100th percentiles, shown in the bottom of the graph as 8 to 195). The radial axis shows wind speed intervals and the colors the probability of having gradient above 88th percentile. This is shown for each bin composed by wind direction and wind speed at 81 m. Plot produced in R with the openair package (Carslaw and Ropkins, 2012)(Carslaw et al., 2010).
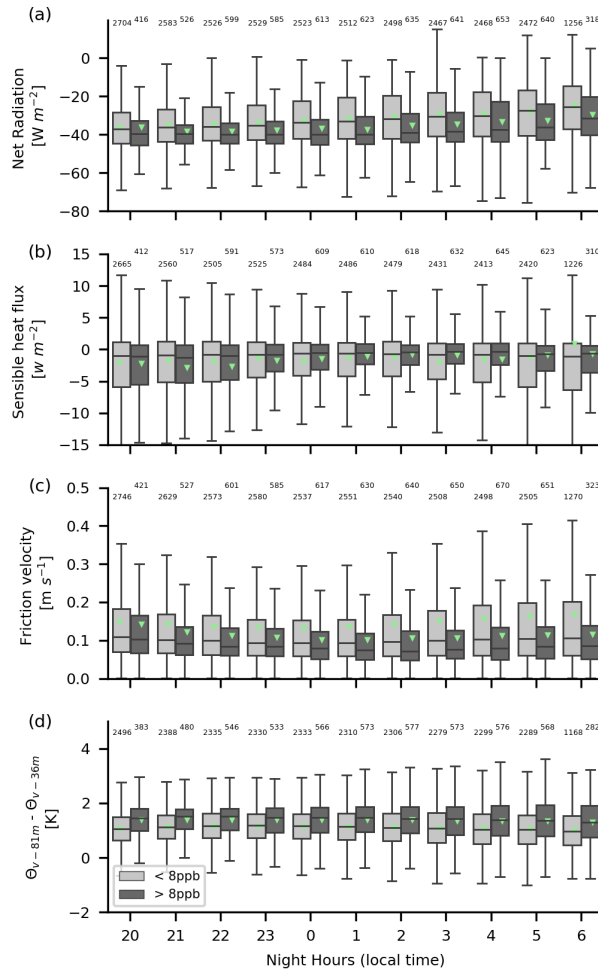
Figure 9. Box-and-whisker plots of net radiation (a), sensible heat flux (b), friction velocity (c), and virtual potential temperature difference (d) for nighttime hours. At each hour the gray colors indicate data points that correspond to either a gradient above 8 ppb or below 8 ppb. The means are indicated by the green triangles and the number of data points for each box-and-whisker plot is shown on the top of each panel. Note that the sensible heat flux and the friction velocity were measured at 81 m and net radiation at 75 m. Note that the air inlet for CH_4 mole ratios is at 79 m.
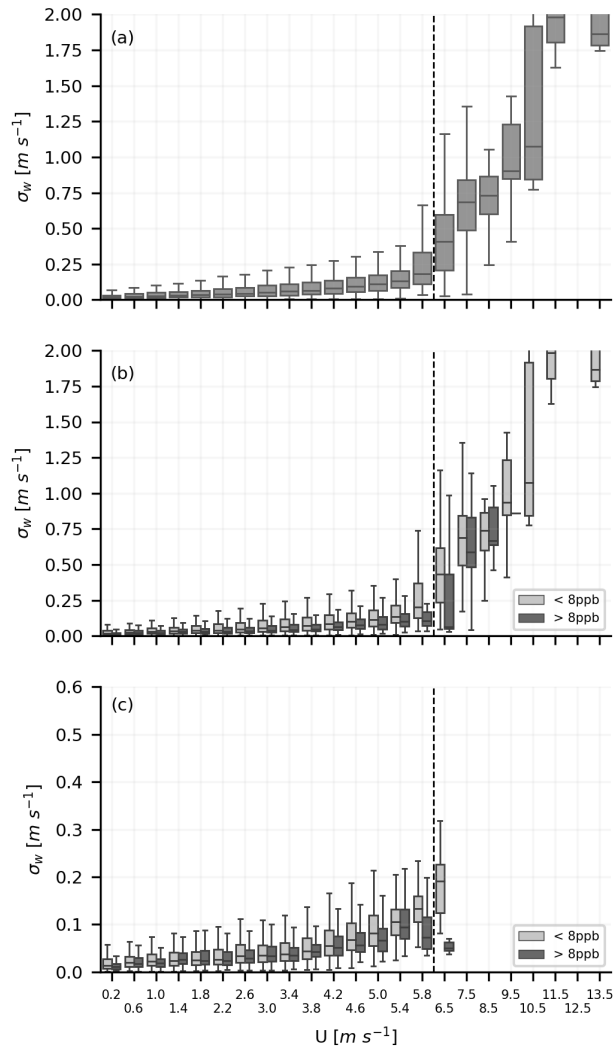
Figure 10. Standard deviation (σ_w) of the vertical velocity, plotted against the mean wind speed, for 1-minute averaging time. ~~In~~ On the top panel (a), the variability of σ_w for each wind speed bin is shown for all data points, with no classification based on CH_4 gradients. On (b), the same as (a) is shown, but ~~the~~ separating between measurements with gradients ~~below and~~ above and below 8 ppb ~~are separated~~. Note that our CH_4 mixing ratio measurements are at 15-minute resolution, therefore we assume the same value ~~for~~ every 15-minute window so we can associate the 1-minute σ_w and U with CH_4 mixing ratios. ~~In~~ On the bottom panel (c), we excluded the 15-minute time periods where the wind speed varied by more than 0.5 ~~m s^{-1}~~ $m\ s^{-1}$. Note the difference in y-axis for (c). The wind speed bins are shown every 0.4 ~~m s^{-1}~~ $m\ s^{-1}$ until 5.8 ~~m s^{-1}~~ $m\ s^{-1}$, after the spacing is 1 ~~m s^{-1}~~ $m\ s^{-1}$. This ~~gradual~~ gradually increase to coarser wind speed bins is done due to ~~sparser~~ less amount of data at higher wind speeds. High-frequency measurements cover six months of 2014: March, April, May, July, August and September.
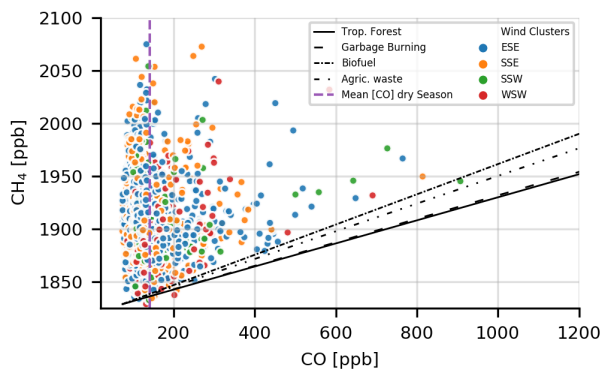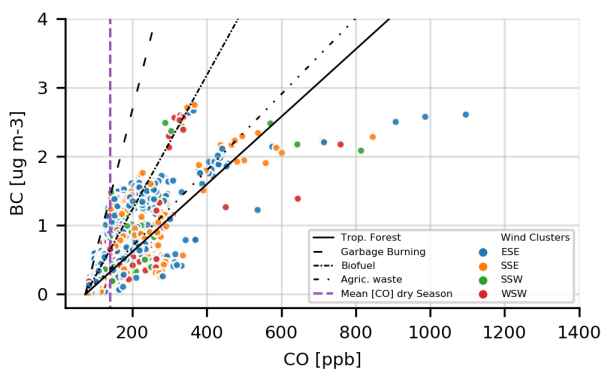
Figure 11. Methane (CH$_4$) as a function of carbon monoxide (CO) together with the slopes of the expected emission ratios (ER) for different types of fires based on the updated assessment of Andreae (2019) and classified into the dominant wind direction clusters for positive gradients (southern quadrants: from 90 to 270 degrees). The data points were filtered to select only nighttime measurements, and the CO data were further filtered to select the same times for which the above-8-ppb class was seen for our CH$_4$ mixing ratio measurements. The data cover the time period between June 2013 and November 2018. All measurements were performed at 79 m.

Figure 12. Black carbon Carbon (BC) as a function of carbon monoxide (CO) together with the slopes of the expected emission ratios (ER) for different types of fires based on the updated assessment of Andreae (2019) and classified into the dominant wind direction clusters for positive gradients (southern quadrants: from 90 to 270 degrees). The data points were filtered to select only nighttime measurements, and the BC data were further filtered to select the same times for periods at which the above-8-ppb class was seen for our CH$_4$ mixing ratio measurements. Note that the time period of these BC data is set spans from 2014 June 2013 to 2015. May 2018. The heights of CO and BC measurements are at 79 m and the BC are at 60 m a.g.l., respectively.
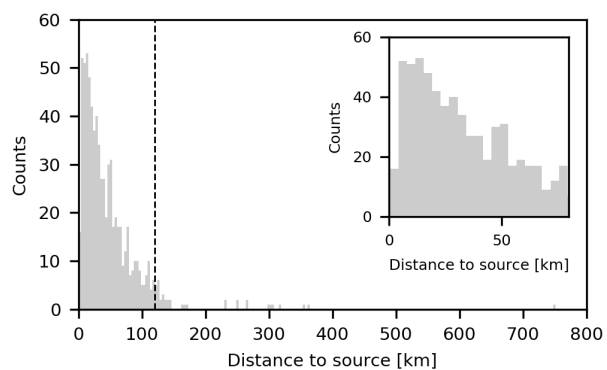
Figure 13. Distribution of the cumulative distance the wind at 81 m travelled from the potential source. The distance was calculated by time-integrating the wind speed at 81 m from 20:00 (beginning of the night) until the first occurrence of a positive gradient (> 8 ppb). The vertical dashed line shows the distance to the Amazon River in the southeast direction. The inset on the top right is a zoomed in view showing the x-axis until 80 km.
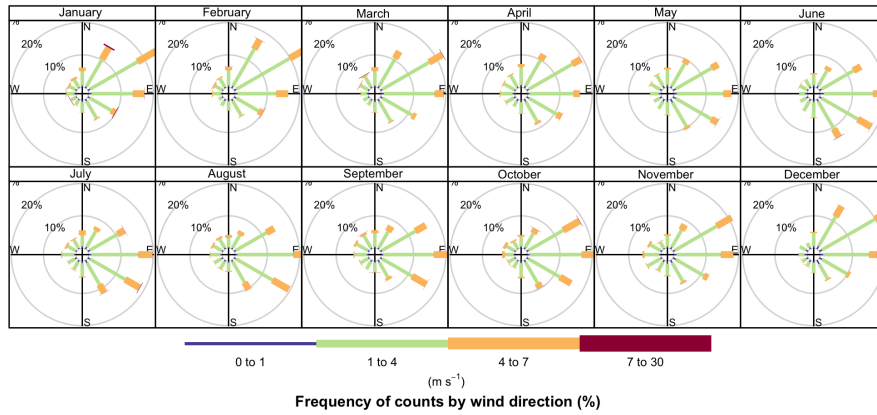
44

Figure A1. Monthly averaged wind rose plots at 81 m.

Appendix A: Mean monthly and mean hourly wind direction

Appendix B: Radiation in wet and dry seasons at ATTO

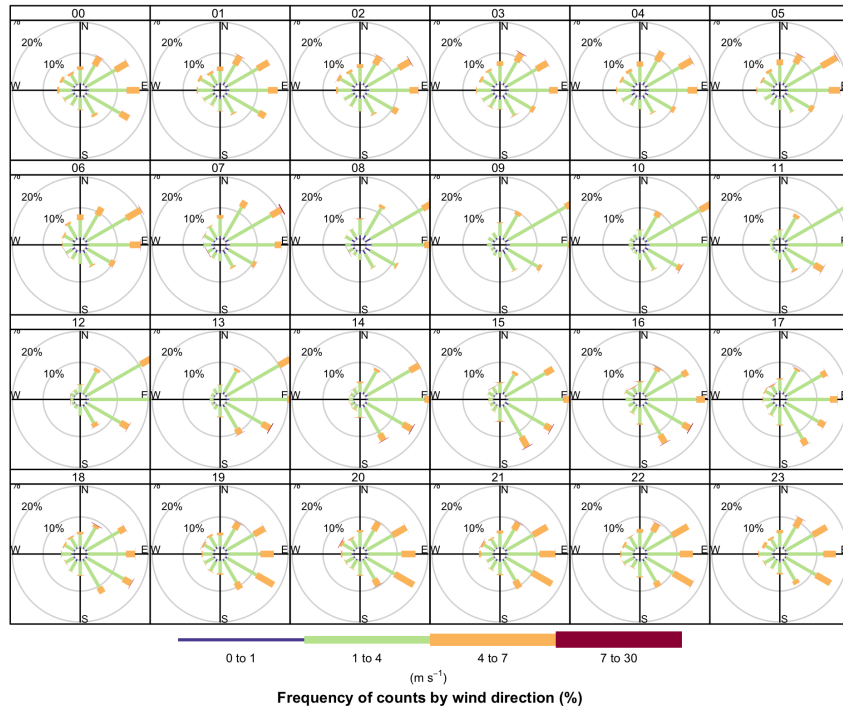**Appendix C: Dead stands of flooded forest**

Figure A2. Hourly mean wind rose plots for each hour of the day. Averaged over all measurement period at 81m.
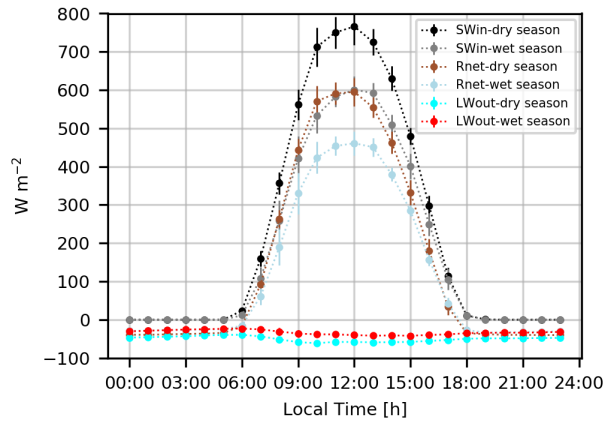

Figure B1. Net, short wave incoming, and long wave outgoing radiation for dry and wet seasons at ATTO.,
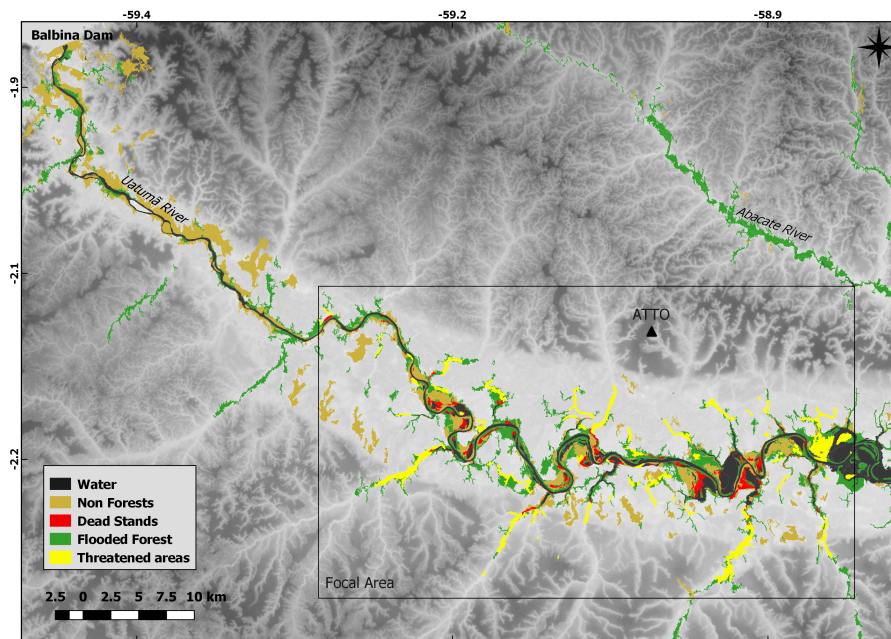
Figure C1. Map showing the dead stands and potentially threatened areas due to the tree mortality caused by the Balbina Dam. This map was modified from Science of The Total Environment, Vol 659, Authors: Angélica Faria de Resende, Jochen Schöngart, Annia Susin Streher, Jefferson Ferreira-Ferreira, Maria Teresa Fernandez Piedade, and Thiago Sanna Freire Silva, Massive tree mortality from flood pulse disturbances in Amazonian floodplain forests: The collateral effects of hydropower production, Pages 587-598, Copyright (2019), with permission from Elsevier.